Global and local curvature in density functional theory

Qing Zhao,[1,2,b)] Efthymios I. Ioannidis,[1,b)] and Heather J. Kulik[1,a)]

[1]*Department of Chemical Engineering, Massachusetts Institute of Technology, Cambridge, MA 02139*

[2]*Department of Mechanical Engineering, Massachusetts Institute of Technology, Cambridge, MA 02139*

Piecewise linearity of the energy with respect to fractional electron removal or addition is a requirement of an electronic structure method that necessitates the presence of a derivative discontinuity at integer electron occupation. Semi-local exchange-correlation (xc) approximations within density functional theory (DFT) fail to reproduce this behavior, giving rise to deviations from linearity with a convex ***global curvature*** that is evidence of many-electron, self-interaction error (SIE) and electron delocalization. Popular functional tuning strategies focus on reproducing piecewise linearity, especially to improve predictions of optical properties. In a divergent approach, Hubbard U-augmented DFT (i.e., DFT+U) treats self-interaction errors by reducing the ***local curvature*** of the energy with respect to electron removal or addition from one localized subshell to the surrounding system. Although it has been suggested that DFT+U should simultaneously alleviate global and local curvature in the atomic limit, no detailed study on real systems has been carried out to probe the validity of this statement. In this work, we show when DFT+U should minimize deviations from linearity and demonstrate that a "+U" correction will never worsen the deviation from linearity of the underlying xc approximation. However, we explain varying degrees of efficiency of the approach over 27 octahedral transition metal complexes with respect to transition metal (Sc-Cu) and ligand strength (CO, NH_3, and H_2O) and investigate select pathological cases where the delocalization error is invisible to DFT+U within an atomic projection framework. Finally, we demonstrate that the global and local curvature represent different quantities that show opposing behavior with increasing ligand field strength, and we identify where these two may still coincide.

I. INTRODUCTION

Density functional theory (DFT) is the workhorse of the electronic structure community, and it is playing an ever increasing role in the design and discovery of new materials[1, 2]. However, presently available exchange-correlation (xc) approximations in DFT are plagued by both one- and many-electron self-interaction errors (SIE)[3-7], which give rise to well-known problems in dissociation energies[4, 8-11], barrier heights[12], band gaps[13, 14], electron affinities[15-17], and other manifestations of delocalization error[18-20]. It has been shown[21] that an exact energy functional

a) Author to whom correspondence should be addressed. Electronic mail: hjkulik@mit.edu.

b) Q. Zhao and E. I. Ioannidis contributed equally to this work.

should be piecewise linear with respect to fractional addition (q) or removal of charge:

$$E(q) = (1-q)E(N) + qE(N+1) \ , \tag{1}$$

where E(N) and E(N+1) are the energies of N- and N+1-electron systems, respectively, and q is varied between 0 (N electrons) and 1 (N+1 electrons). This piecewise linearity[22] necessitates a derivative discontinuity[23-26] in an exact functional, but the analytical forms of common xc approximations lack this discontinuity unless re-expressed in an ensemble formalism[27, 28]. Instead, both semi-local (e.g., generalized gradient approximation, GGAs) functionals and the formally self-interaction free Hartree-Fock (HF) theory produce a deviation from linearity in E(q) with convex and concave behavior, respectively.[3, 29] We refer to the second derivative of the energy with respect to charge, $\frac{\partial^2 E}{\partial q^2}$, as a ***global curvature*** that is a good measure of a functional's delocalization error and energetic deviation from linearity.

Utilizing Janak's[30] or Koopmans'[31] theorem, Stein et al.[32] showed that an average or constant ***global curvature*** of a functional may be approximated as the difference in the N+1-electron highest occupied molecular orbital (HOMO) and the N-electron lowest unoccupied molecular orbital (LUMO) eigenvalues:

$$\left\langle \frac{\partial^2 E}{\partial q^2} \right\rangle = \varepsilon_{N+1}^{\mathrm{HOMO}} - \varepsilon_{N}^{\mathrm{LUMO}} \ . \tag{2}$$

In the same work[32], Stein et al. also proposed a linear-response approach to obtaining the curvature, as outlined in the Supporting Information of Ref. [32]. By tuning the range separation parameters[33-42] that divide short-range semi-local or hybrid xc forms from long-range HF exchange to minimize this curvature, long-range corrected (LRC) hybrids[43-49] frequently improve

excited state[50] and some ground state[37] properties by improving delocalization or self-interaction error[3, 6, 13, 19, 20, 39, 51, 52]. Similar efforts have motivated xc functionals[53-55] that explicitly obey Koopmans' theorem[31] and the improvement of approaches in many-body perturbation theory (i.e., GW)[56]. However, the curvature-minimizing strategy is not without issues, occasionally worsening predictions[57-60] and showing marked size-dependence[57, 58, 61, 62]. Such size-dependence suggests that deviation from linearity is not sufficient for identifying SIE-free electronic structure methods, as it only guarantees removal of relative errors with respect to integer-electron endpoints and makes the likely incorrect assumption that what we will refer to as endpoint error (i.e., delocalization error effects on the total energy at integer electron number) is not increasing with system size. Orbital-dependent self-interaction corrections have also been pursued for some time[63-68], but curvature-correction through optimally-tuned hybrid functionals remains the most widely employed SIE-correction strategy due to the relative ease of use and broad applicability of range-separated hybrids.

The self-consistent, linear-response DFT+U method shares similarities in spirit to LRC hybrid tuning but is applied much more frequently in solid-state transition-metal-containing materials, where long-range exchange remains more computationally expensive than semi-local xc approximations. Within DFT+U, the ***local curvature*** of the energy with respect to addition or removal of electrons from a localized subshell (n_{nl}^{I}) to the rest of the system at constant charge is minimized, and the calculated Hubbard U, or ***local curvature***, is:

$$U_{nl}^{I} = \left.\frac{\partial^2 E}{\partial (n_{nl}^{I})^2}\right|_{q} \quad . \tag{3}$$

This ***local curvature*** is obtained from the second derivative of the energy with respect to occupations on a single atom *I* computed at a constant charge, *q*, whereas ***global curvature*** is the

second derivative of the energy with respect to total charge, q, of the overall system. A main motivation for the DFT+U approach is the recognition that its functional form should also exactly recover piecewise linearity for an atom as fractional charge is added or removed to a localized subshell as long as global curvature is constant and $\delta n \propto \delta q$ (Figure 1). However, there is no reason that the two curvatures should necessarily be equal, since the ***global curvature*** reflects the behavior of the energy upon electron removal or addition, whereas the U, which we refer to here as the ***local curvature***, reflects the change in energy as an electron is redistributed to the rest of the system. Furthermore, it has been argued[69, 70] that if the nl subshell orbitals treated with DFT+U are frontier orbitals, the derivative discontinuity may be recovered, alleviating band gap problems within semi-local DFT because the DFT+U potential shifts orbitals with opposing character differently (see Sec. II). Notably, if the frontier orbitals do not have sufficient nl subshell character, then DFT+U may have little or no effect on the semi-local DFT band gap. In practice, DFT+U is widely used to address delocalization at integer occupations, i.e., endpoint total energy error in the ground state, which is different in spirit from the LRC approach that focuses on excitation energies. However, it is worthwhile to investigate whether deviation from linearity errors can also simultaneously be addressed by DFT+U in real systems.

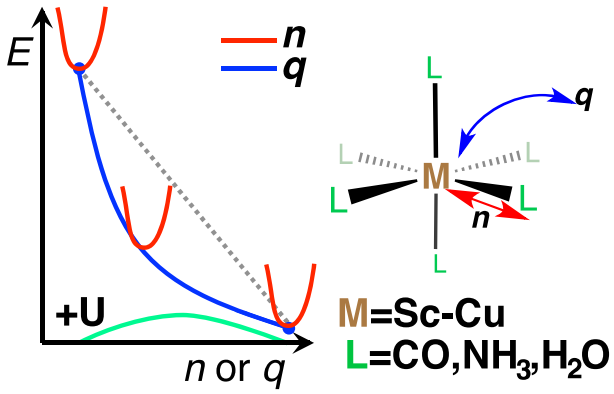

Figure 1. (Left) Comparison of the dependence of the energy in a practical exchange-correlation functional (e.g. GGA) as the charge (q) is varied between integer points (blue lines) with the energy as on-site occupations (n) are varied at a fixed q (red lines) along with representative

correct piecewise linear behavior (gray dashed line). An example +U correction is shown in the atomic limit (green line). (Right) Octahedral metal-ligand complexes studied in this work (inset) with a schematic showing that n is varied for fixed q by shifting electrons between the metal and surrounding environment as compared to complete electron removal, which also affects n.

We thus present the first such investigation of the theoretical limits of DFT+U for global curvature corrections by focusing on model electron configurations in Sec. II. Computational details are summarized in Sec. III. In Sec. IV, we present and discuss results on calculated properties of 27 transition metal complexes to identify the extent DFT+U eliminates deviations from linearity in practice, and we also identify the relationship between global E vs. q and local U curvature. Finally, we provide our Conclusions in Sec. V.

II. THEORY

Beyond average curvature expressions[32], Johnson and coworkers have demonstrated[20] that the energetic behavior of semi-local and hybrid functionals with fractional charge can be interpolated using quantities obtained only at integer electron count with the following cubic spline equation:

$$E(q) = \Delta E q + [(\varepsilon_N^{\mathrm{LUMO}} - \Delta E)(1-q) + (\Delta E - \varepsilon_{N+1}^{\mathrm{HOMO}})q]q(1-q), \quad (4)$$

where q = 0 and 1 correspond to the N- and N+1-electron systems, respectively. Here, ΔE is the difference in energy between the N+1- and N-electron molecules:

$$\Delta E = E(N+1) - E(N). \quad (5)$$

The N-electron LUMO eigenvalue, $\varepsilon_N^{\mathrm{LUMO}}$, and N+1-electron HOMO eigenvalue, $\varepsilon_{N+1}^{\mathrm{HOMO}}$, are incorporated into the fit as they approximate the first derivative of the energy with respect to electron removal or addition[30]. We focus on the deviation from linearity at any value of q:

$$E^{\mathrm{dev}}(q) = E(q) - \Delta E q = [(\varepsilon_N^{\mathrm{LUMO}} - \Delta E)(1-q) + (\Delta E - \varepsilon_{N+1}^{\mathrm{HOMO}})q]q(1-q), \quad (6)$$

which highlights that deviations from linearity, $E^{\mathrm{dev}}(q)$, disappear when the LUMO of the N-electron system and HOMO of the N+1-electron system faithfully represent the N-electron electron affinity (EA) and N+1-electron ionization potential (IP), respectively. Semi-local DFT is well known to exhibit convex behavior, i.e. negative $E^{\mathrm{dev}}(q)$ for q between 0 and 1.[3, 29]

An alternative approach to improve delocalization error in molecules and solids is the so-called DFT+U method[71-74]. Within DFT+U, a Hubbard model Hamiltonian correction is added to a standard xc approximation to tune the degree of localization of electrons on specific Hubbard atoms. A frequent argument[70, 75] for the theoretical rigor of DFT+U has been that within the atomic limit, the functional form of DFT+U corrects parabolic global curvature errors at fractional charge. When DFT+U is in applied to systems that exhibit hybridization and delocalization with surrounding atoms, the effect of DFT+U on global curvature errors is not known. We now examine the "+U" functional form and how it may alter E^{dev} as predicted via the cubic spline expression of Johnson and coworkers[20].

First, recall that the full DFT+U energy functional[71, 73] is:

$$E_{\mathrm{DFT+U}}[n(\mathbf{r})] = E_{\mathrm{DFT}}[n(\mathbf{r})] + E_{\mathrm{Hub}}[\{n_m^{I\sigma}\}] - E_{\mathrm{DC}}[\{n^{I\sigma}\}]\,, \tag{7}$$

where the first term (DFT) is the contribution from a standard xc approximation, the second term (Hub) is a Hubbard model Hamiltonian correction, and the double counting (DC) term approximately removes the effect of corrections present in both of the first two terms. There will be a Hub and DC contribution for each Hubbard atom and subshell identified. Most commonly, the DC term is obtained within the fully-localized limit:

$$E_{\mathrm{DC}}[\{n^{\sigma}\}] = \frac{1}{2}Un(n-1) - \frac{1}{2}J[n^{\uparrow}(n^{\uparrow}-1) + n^{\downarrow}(n^{\downarrow}-1)], \tag{8}$$

where the total number of electrons is denoted n, spin up or down electrons is denoted $n^{\uparrow}$ or $n^{\downarrow}$, respectively.

A frequent simplifying assumption[75, 76] is to treat same-spin and opposite-spin electrons equivalently with $U_{\text{eff}}=U-J$, yielding an expression for the DFT+U energy as:

$$E^{\text{DFT+U}} = E^{\text{DFT}} + \frac{1}{2}\sum_{I,\sigma}\sum_{nl} U^{I}_{nl}[\text{Tr}(\mathbf{n}^{I\sigma}_{nl}(\mathbf{1}-\mathbf{n}^{I\sigma}_{nl})] \ . \tag{9}$$

There is a "+U" contribution for each nl subshell of atom I to which a U^{I}_{nl} is applied. The elements of the $\mathbf{n}^{I\sigma}_{nl}$ occupation matrix are obtained as a projection of the molecular state $\left|\psi_{k,v}\right\rangle$ at k-point k onto localized atomic orbitals on an atom I:

$$n^{I\sigma}_{mm'} = \sum_{k,v}\left\langle \psi_{k,v}\middle|\phi^{I}_{m'}\right\rangle\left\langle \phi^{I}_{m}\middle|\psi_{k,v}\right\rangle \ . \tag{10}$$

The "+U" correction is incorporated self-consistently with a modification to the potential as:

$$V^{U} = \sum_{I,nl}\sum_{m}\frac{U^{I}_{nl}}{2}(1-2n^{I\sigma}_{nl,m})\left|\phi^{I}_{nl,m}\right\rangle\left\langle\phi^{I}_{nl,m}\right| \ , \tag{11}$$

where the shifts are a maximum $U/2$ or minimum $-U/2$ for molecular orbitals (MOs) that project fully onto the atomic orbitals (AOs) that are empty or filled, respectively.

The Hubbard U in these DFT+U corrections corresponds to the difference between the IP and EA of electrons on atom I in subshell nl with respect to the rest of the system:

$$U^{I}_{nl} = \text{IP}^{I}_{nl} - \text{EA}^{I}_{nl} = E(n^{I}_{nl}+1) + E(n^{I}_{nl}-1) - 2E(n^{I}_{nl}) \ , \tag{12}$$

which may be recognized as a finite difference approximation to the second derivative of the

energy (i.e., $U_{nl}^{I} = \frac{\partial^2 E}{\partial (n_{nl}^{I})^2}$). More details on calculating[75, 77] U are outlined in the Appendix.

The simple functional form of DFT+U enables us to directly identify the manner in which a "+U" correction alters the E^{dev} of an underlying xc approximation as:

$$\frac{\partial E^{\text{dev}}(q)}{\partial U} = \left[\left(\frac{\partial \varepsilon_N^{\text{LUMO}}}{\partial U} - \frac{\partial \Delta E}{\partial U} \right)(1-q) + \left(\frac{\partial \Delta E}{\partial U} - \frac{\partial \varepsilon_{N+1}^{\text{HOMO}}}{\partial U} \right) q \right] q(1-q) \ . \tag{13}$$

Here, we will distinguish LUMO error (LE) as the deviation from linearity arising from the first term inside the brackets, whereas the HOMO error (HE) is the deviation from linearity arising from the second term in eqn. 13. Due to the order of subtraction and sign convention, both the HE and LE are negative numbers. If the DFT+U functional is successful in reducing convexity in the underlying exchange-correlation approximation, then $\frac{\partial E^{dev}(q)}{\partial U}$ will be positive as a result of positive first derivatives of both the HE and LE with U.

Both the HE and LE derivatives with U incorporate the derivative $\frac{\partial \Delta E}{\partial U}$, which is:

$$\frac{\partial \Delta E}{\partial U} = \frac{\partial E(N+1)}{\partial U} - \frac{\partial E(N)}{\partial U} \ , \tag{14}$$

where we make the approximation to the low-U-limit that the only change in the energy with U is due to the "+U" component of the functional and there is no change in the underlying xc approximation energy of the N+1- and N-electron systems with applied U. Then, we can express in terms of the respective occupation matrices of the N+1- and N-electron states:

$$\frac{\partial \Delta E}{\partial U} = \frac{\partial}{\partial U}\left(\frac{U}{2} \text{Tr}\left[\mathbf{n}_{N+1}(\mathbf{1} - \mathbf{n}_{N+1}) \right] \right) - \frac{\partial}{\partial U}\left(\frac{U}{2} \text{Tr}\left[\mathbf{n}_{N}(\mathbf{1} - \mathbf{n}_{N}) \right] \right), \tag{15}$$

where $\mathbf{n}_{N+1}$ and $\mathbf{n}_N$ represent the occupation matrices of the *N*+1- and *N*-electron systems, respectively, and the $\mathrm{Tr}\left[\mathbf{n}(\mathbf{1}-\mathbf{n})\right]$ term is the fractionality of the system.[78]

When adding an electron to the *N*-electron system, up to 100% of that electron will manifest in larger values of elements in the occupation matrix of the *N*+1-electron system. Working in a diagonal occupation basis enables us to directly cast *N*+1- and *N*-electron fractionality differences in terms of projected AO filling differences. An occupation matrix element of the *N*+1-electron system becomes $n_{mm}^{I\sigma}$, where *I* and σ are atomic the site and spin, and the *mm* subscript indicates the diagonal element of the occupation matrix with quantum number m_l=m. Then the *N*-electron system occupation matrix elements are $n_{mm}^{I\sigma}-\Delta n_{mm}^{I\sigma}$, where $0\le\Delta n_{mm}^{I\sigma}\le n_{mm}^{I\sigma}\le 1$. The "+U"-derived energy difference of the two states (ΔE^U) becomes:

$$\Delta E^U=\frac{U}{2}\left(\sum_m n_{mm}-n_{mm}^2-(n_{mm}-\Delta n_{mm})+(n_{mm}-\Delta n_{mm})^2\right), \tag{16}$$

where the first two terms comprise the fractionality of the *N*+1-electron system and the last two the *N*-electron system fractionality. We simplify ΔE^U by defining and extracting the total occupation shift, $\Delta n_{\mathrm{tot}}=\sum_m \Delta n_{mm}$:

$$\Delta E^U=\frac{U}{2}\left[\Delta n_{\mathrm{tot}}+\sum_m \Delta n_{mm}\left(\Delta n_{mm}-2n_{mm}\right)\right]. \tag{17}$$

The term in the inner parentheses must always be negative, and the expression will be most negative if the addition or removal of the electron is well-localized to a single element of the occupation matrix (i.e., $1\sim\Delta n_i >> \Delta n_{j\neq i}$). We further simplify by assuming that the MO being

emptied or filled projects onto a single AO, leading to the simplified $\frac{\partial \Delta E}{\partial U}$ derivative:

$$\frac{\partial \Delta E}{\partial U} = \frac{1}{2}\left[\Delta n + \Delta n^2 - 2n\Delta n\right], \tag{18}$$

where we have dropped all subscripts on the occupation matrix element and shift to indicate that only a single level is involved. Limits in this simplified expression are clear: if the N+1-electron state is maximally fractional (i.e., n=½) and this ½ electron is fully removed during ionization to the neutral case, then the change in energy shift with U is a maximally positive value of 0.125 eV/eV of U. For a minimally-fractional (i.e., n=1) N+1 state with ½ electron removal, the change in energy shift with U is maximally negative at -0.125 eV/eV (see Figure 2c). If the two states have equivalent fractionality, e.g. $n = \Delta n = 1, n = \Delta n = 1$ then ΔE is unchanged with U.

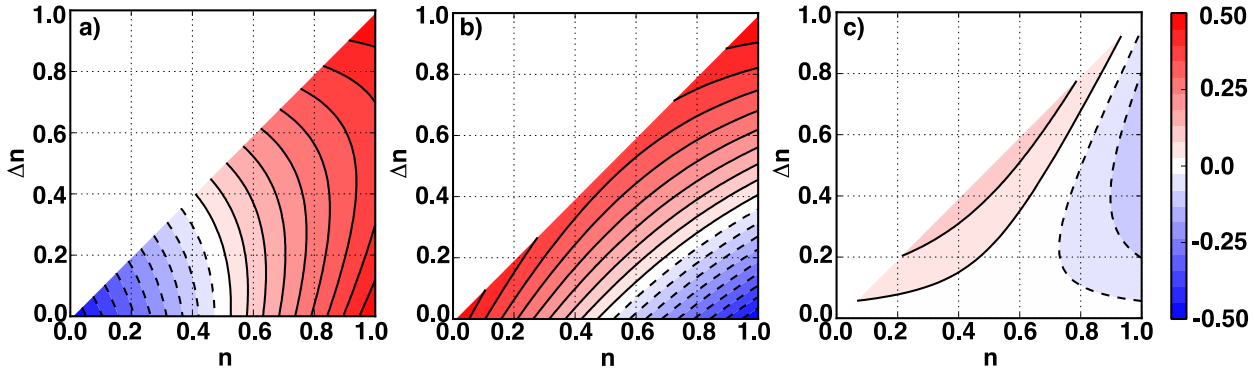

Figure 2. a) Dependence of HOMO error derivative with U in eV/eV on the N+1-electron system occupation (n) and the fractional occupation loss (Δn). b) Dependence of LUMO error derivative with U in eV/eV on the N+1-electron system occupation (n) and the fractional occupation loss (Δn). c) Dependence of only the anion-neutral energy difference (ΔE) on U in eV/eV on the N+1-electron system occupation (n) and fractional occupation loss (Δn). All three plots employ the same color gradient with color bar shown at right ranging from -0.5 eV/eV (blue) to +0.5 eV/eV (red).

We will now show that the derivative of the eigenvalues with respect to applied U value contributes more strongly to shifts in HE and LE than the energy shift. These eigenvalue energy derivatives are closely related to the DFT+U potential as:

$$\frac{\partial \varepsilon}{\partial U} = \left\langle \psi_{k,\nu} \middle| \frac{\partial V^U}{\partial U} \middle| \psi_{k,\nu} \right\rangle \ , \tag{19}$$

where $\frac{\partial V^U}{\partial U}$ is the non-vanishing Hubbard contribution to the potential. We again neglect any higher-order contributions, e.g. from the "+U" correction changing the density. Recall, the derivative of the "+U" contribution to the potential with respect to U is:

$$\frac{\partial V^U}{\partial U} = \frac{1}{2} \sum_{I,m} (1 - 2n_m^{I\sigma}) \left| \phi_m^I \right\rangle \left\langle \phi_m^I \right| \ . \tag{20}$$

This potential term produces an eigenvalue shift with U as:

$$\frac{\partial \varepsilon_{k,\nu}}{\partial U} = \left\langle \psi_{k,\nu} \middle| \frac{1}{2} \sum_{I,m} (1 - 2n_m^{I\sigma}) \left| \phi_m^I \right\rangle \left\langle \phi_m^I \middle| \psi_{k,\nu} \right\rangle \right. \ , \tag{21}$$

where we recognize the projection of the k-,ν-indexed MO onto the AO that contribute to the eigenvalue shift. This projection may be rewritten as a new occupation term:

$$n_{m,k\nu}^{I\sigma} = \left\langle \psi_{k,\nu} \middle| \phi_m^I \right\rangle \left\langle \phi_m^I \middle| \psi_{k,\nu} \right\rangle \ , \tag{22}$$

and the eigenvalue dependence on U may be written in terms of these two occupations as:

$$\frac{\partial \varepsilon_{k,\nu}}{\partial U} = \frac{1}{2} \sum_{I,m} (1 - 2n_m^{I\sigma}) n_{m,k\nu}^{I\sigma} \ . \tag{23}$$

Two factors thus determine the extent of eigenvalue shift with U: i) the MO must have a strong contribution from one of the projected basis AOs and ii) the AOs should have near integer (i.e., 0 or 1) occupations. These multiplicative effects (eqn. 23 is plotted in Figure 3) lead to fast attenuation of the effect of DFT+U on an eigenvalue if i) the AO occupation decreases through

hybridization or ii) the contribution of the AO to the MO diminishes. In the limit of an MO projecting exactly onto one AO, the appropriate simplified eigenvalue shift becomes:

$$\frac{\partial \varepsilon}{\partial U} = \frac{1}{2}(1 - 2n^{\text{occ}}) \,, \tag{24}$$

where n^{occ} is the occupations of the relevant AO. In the fully unoccupied and occupied limits, the potential shift becomes maximally positive (0.5 eV/eV of U) or negative (-0.5 eV/eV of U), respectively, which is 4x the maximum $\frac{\partial \Delta E}{\partial U}$ in the HE/LE correction (Figure 3). Unoccupied MOs are often diffuse, making the maximum positive shift likely harder to achieve (see Sec. IV).

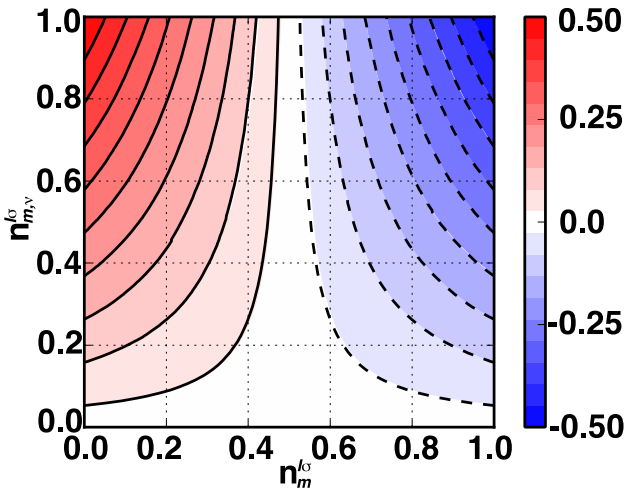

Figure 3. Rate of change of a molecular orbital energy with U based on the occupation of the orbital in the molecular orbital ($n_{m,\nu}^{I\sigma}$) and the occupation of that atomic orbital ($n_m^{I\sigma}$), for both occupied and unoccupied MOs. The data ranges from -0.50 eV/eV in blue to +0.50 eV/eV in red, as indicated by color bar in inset.

The resulting formulae for LE and HE in the single orbital-emptying and filling limit are:

$$\frac{\partial \text{LE}}{\partial U} = \frac{\partial \varepsilon_N^{\text{LUMO}}}{\partial U} - \frac{\partial \Delta E}{\partial U} = \frac{1}{2}[1 - 2(n - \Delta n)] - \frac{1}{2}\left(\Delta n + \Delta n^2 - 2n\Delta n\right) \text{, and} \tag{25}$$

$$\frac{\partial \mathrm{HE}}{\partial U} = \frac{\partial \Delta E}{\partial U} - \frac{\partial \varepsilon_{N+1}^{\mathrm{HOMO}}}{\partial U} = \frac{1}{2}\left(\Delta n + \Delta n^2 - 2n\Delta n\right) - \frac{1}{2}(1-2n) \ . \tag{26}$$

These expressions reveal that maximum HE reduction occurs when a fully occupied orbital is emptied, but n> ½ all reduce HE (Figure 2a). The LE shift is positive over a more stringent range of occupations in the *N*+1- and *N*-electron states due to the competing effects of the eigenvalue and energy shift terms. Even when the *N*+1-electron state is well-occupied (i.e., $0.6 \le n \le 1$), the LE increases for $\Delta n \le 0.4$. Low *n* can yield productive LE shifts but must be emptied (i.e., n~Δn, Figure 2b), emphasizing high sensitivity of the LE to the dominant AO in the LUMO.

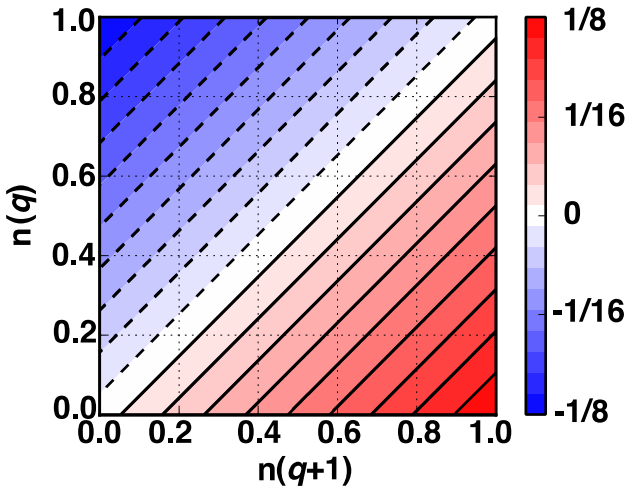

Figure 4. Rate of change of E^{dev} with *U* at *q*=+½ in eV/eV based on the occupation of the emptying or filling orbital for the *N*+1- (*q*=1) and *N*- (*q*=0) electron states, respectively. The data ranges from -0.125 eV/eV in blue to +0.125 eV/eV in red, as indicated by color bar in inset.

A typical assumption is that the deviation from linearity has a maximum value at *q*=1/2 where, conveniently, the E^{dev} cubic spline and its derivative with *U* simplifies to:

$$\left.\frac{\partial E^{\mathrm{dev}}(q)}{\partial U}\right|_{q=1/2} = \frac{1}{8}\left(\frac{\partial \varepsilon_N^{\mathrm{LUMO}}}{\partial U} - \frac{\partial \varepsilon_{N+1}^{\mathrm{HOMO}}}{\partial U}\right) \ . \tag{27}$$

The E^{dev} shift with *U* at q=1/2 depends only on the *N*+1- and *N*-electron frontier orbital energy

shifts with U. We identified that the maximum negative/positive shift occurs when an MO projects onto one occupied/unoccupied AO. In this limit, the eqn. 27 simplifies to:

$$\left.\frac{\partial E^{dev}(q)}{\partial U}\right|_{q=1/2} = \frac{1}{16}\{[1-2(n-\Delta n)]-(1-2n)\} = \frac{\Delta n}{8}, \quad (28)$$

where $0<\Delta n<n$ and $0<n<1$, and a maximum 0.125 eV/eV derivative is achieved for n=1 and Δn=1 (Figure 4). If the occupations do not shift (i.e., Δn=0), then the "+U" correction will have no effect. Only in the highly unlikely case that the occupations of the N-electron reference are higher than the N+1-electron reference would a "+U" correction increase E vs. q convexity. This observation highlights the potential benefit of a negatively valued U in HF+U, which we have previously discussed[79] and found beneficial to employ[78] to correct HF problems with concave, overlocalization. We next investigate whether the DFT+U curvature corrections to real inorganic complexes achieve the best case, limiting scenarios identified and whether the maximum E^{dev} correction is sufficient to correct convexity in semi-local xc approximations (see Sec. IV).

III. COMPUTATIONAL DETAILS

Calculations on 28 M(II)/M(III) octahedral complexes (Sc-Cu with H_2O, NH_3, and CO ligands as well as Zn with H_2O ligands) and the iron atom were carried out using the plane-wave periodic boundary condition code Quantum-ESPRESSO[80]. The Perdew-Burke-Ernzerhof (PBE)[81] generalized-gradient approximation (GGA) was employed with ultrasoft pseudopotentials (USPPs)[82] obtained from the Quantum-ESPRESSO website[83]. Plane wave cutoffs for the USPPs employed were 30 Ry for the wavefunction and 300 Ry for the charge density. For Sc, Ti, V, Cr, Mn, and Fe, USPPs with semicore 3*s*/3*p* states in the valence were used, and. for Co, Ni, Cu, and Zn, only the 3*d* and 4*s* states were in the valence. Rappe-Rabe-Kaxiras-Joannopoulos USPPs[84] were employed for carbon, hydrogen, oxygen, and nitrogen in

the test set ligands. A complete list of all USPPs used in this work is provided in supplementary material Table S1. In order to eliminate periodic image effects in the calculations on the molecular complexes studied, the Martyna-Tuckerman scheme[85] was used along with substantial vacuum inside the 14.8 Å cubic box. At least 15 and up to 25 unoccupied states (bands) were included for all complexes. All optimized geometries are provided in the supplementary material.

Initial structures were built with the molSimplify[86] toolkit with both ligand force-field preoptimization and trained metal-ligand bond lengths features enabled. These structures were subsequently geometry optimized with PBE-GGA in the +3 charge state, which was taken as the *N*-electron reference. Any additional calculations of other charge states were obtained on that optimized geometry, regardless of differences in charge or *U* value employed. Fractional electron calculations were carried out by manually altering band occupations using the 'from_input' command in Quantum-ESPRESSO.

Except for the low-spin $Fe(CO)_6$ case, the ground state spin of the isolated atom, as obtained from the National Institute of Standards and Technology atomic spectra database[87], was employed for all studies to simplify ligand-field-dependent comparisons. This spin state choice is likely correct for the weak field, hexa-aqua complexes, but a low-spin state may be preferred for strong field carbonyl ligands, with spin states of the ammonia complexes likely being metal- and xc-approximation-dependent[88, 89]. For the nine metals studied, M(II/III) complexes range from nominally d^1/d^0 for Sc to d^9/d^8 for Cu. The +2/+3 redox states are considered here due to their prevalence in biological and inorganic catalytic cycles[90] and due to their nominal 3*d* occupation difference. From Sc to Mn, the M(II)/M(III) spin state increases from doublet and singlet for Sc to sextet and quintet for Mn, as a majority spin electron added. For Fe to Cu, spin states are reversed with M(II) and M(III) Fe corresponding to quintet and sextet and decreasing magnetic

moment down to doublet and triplet for Cu, as a minority spin electron is added.

Linear response U calculations[75, 91] were carried out using a rigid potential shift ranging from -0.2 eV to +0.2 eV in roughly 0.02 eV increments. In select cases, difficulties converging the GGA ground state necessitated calculation of a self-consistent U on the DFT+U density instead.[77] A standard, linear-response calculation of U was employed for the remaining cases due to previous observations[92] that the two coincide for cases where the GGA and +U electronic states are qualitatively the same. For fractional charge linear response U calculations, the same procedure was applied for linear-response U calculation but with a non-integer total charge. Density difference and molecular orbital density isosurfaces were plotted at ± 0.002 e-.

IV. RESULTS AND DISCUSSION

A. Validating Interpolated *E* vs. *q* within DFT+U

It is expedient to employ the interpolated formula suggested and demonstrated on semi-local DFT total energies by Johnson and coworkers[20], but it is not yet clear that the correspondence will hold for DFT+U total energies of molecules. In the limit of a single atomic orbital filled or emptied as charge is varied, it is evident that the fractionality will smoothly vary, but for molecules, solids, and atoms with degenerate orbitals, the added fractional electron could hybridize differently over a number of already fractionally occupied orbitals at different q.

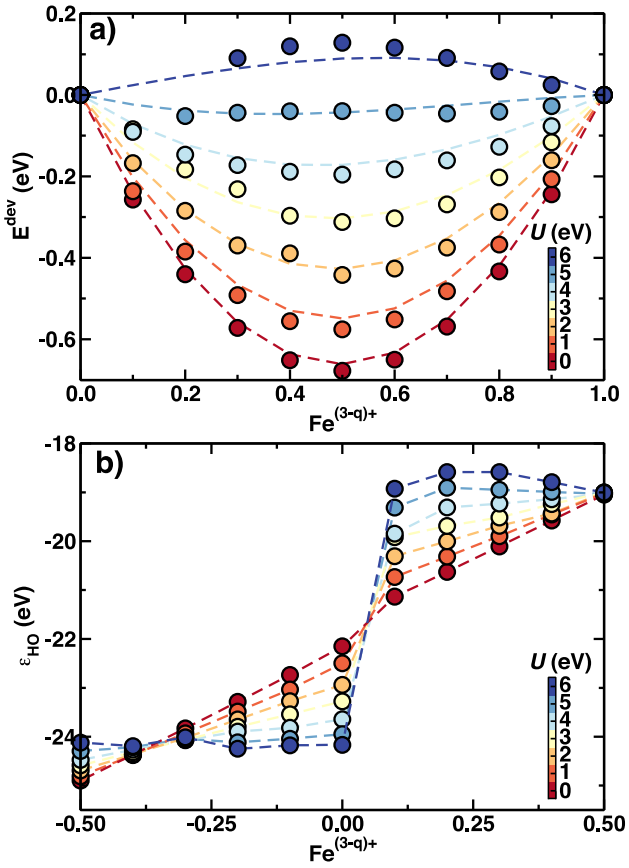

Figure 5. a) Comparison of real (circle symbols) and interpolated (dashed lines) deviation from linearity (E^{dev}) for low-spin $Fe(CO)_6$. b) Highest-occupied eigenvalue (ε_{HO}) with charge centered around $Fe(CO)_6^{3+}$. The lines for both graphs are colored by the value of U applied following the color bar shown in inset (i.e., red is a pure GGA result and blue is a U = 6 eV result).

However, we do indeed find the interpolated cubic spline holds for predicting DFT+U E^{dev}, as shown for a low-spin $Fe(CO)_6$ complex (Figure 5a).For the larger U values at which we approach linearity, multiple solutions may emerge[92-94] giving some rise to noisiness in the fractional energies, but overall fidelity between the interpolation and calculated values is quite good (see supplementary material Figures S1-8 for results on eight other complexes). The E^{dev} crosses from convex to concave at U = 5-6 eV, which are typical values applied in DFT+U calculations. The starting E^{dev} of -0.7 eV at q=+0.5 is thus reduced by nearly the maximum theoretical limit we identified of 0.125 eV/eV of U (see Sec. IV.C for broader efficiency

discussion). Both the real and interpolated data provide the first evidence that DFT+U is suitable to alleviate global curvature errors even in systems with considerable hybridization. As expected, the derivative discontinuity (Figure 5b) is also restored as determined by the eigenvalue of the highest-occupied level (ε_{HO}) within $q \pm 0.5$ of the +3 charge state. Invariant eigenvalues with MO filling are observed around U = 5-6 eV, consistent with the energy perspective.

B. DFT+U corrections to convexity

We now compare components of the validated spline for five representative complexes to identify how "+U" corrections reduce deviation from linearity (Figure 6). The GGA HEs and LEs are comparable around -2.5 and -4.0 eV and produce maximum E^{dev} GGA values that range from -1.0 to -0.7 eV. Recall, HEs and LEs are both negative from sign convention but arise due to the N+1-electron HOMO energy being too high and the N-electron LUMO being too low. The "+U" correction has a consistent effect on most of the complexes compared. As suggested in Sec. II, energy differences between N- and N+1-electron states become slightly more negative as U is increased for 4 of the 5 complexes, especially for hexa-aqua iron. Low-spin iron hexa-carbonyl is the sole exception in which the energy difference decreases as U is increased. In all iron complexes, HEs and LEs are reduced as U is increased with comparable slopes in LE and HE reduction leading to a projected linearity around U = 5-8 eV. In contrast to iron, $Mn(CO)_6$ HOMO and LUMO errors are nearly unchanged as U is increased, and this reduced efficiency as well as in the hexa-aqua complex will be revisited in Sec. IV.C. Based on the theoretical model that we introduced in Sec. II, unchanging $Mn(CO)_6$ HE and LE suggests unchanged, half-filled AO associated with both frontier orbitals. In most cases, DFT+U alleviates deviation from linearity by eliminating HEs and LEs through HOMO stabilization and LUMO destabilization along with a secondary effect on ΔE.

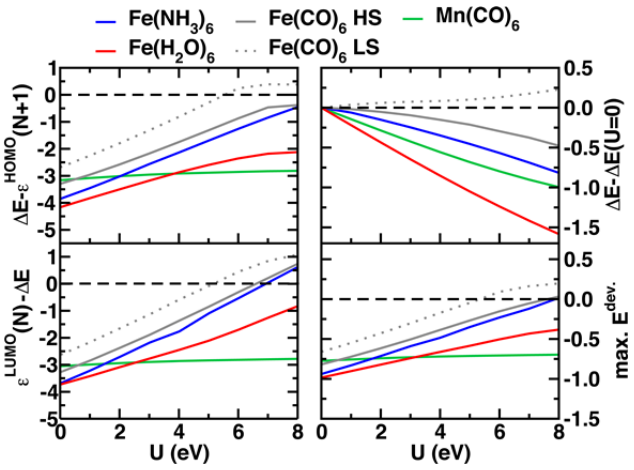

Figure 6. Comparison of deviation from linearity components and their dependence on *U* value in eV for four iron octahedral complexes with differing ligands and spins (NH_3 in blue, H_2O in red, CO high-spin in gray solid and CO low-spin in gray dashed lines) with one manganese octahedral complex (CO in green). Specifically, we compare the HOMO error (top, left), LUMO error (bottom, left), shift in energy difference (top, right), and total maximum deviation from linearity (bottom, right) all in units of eV. The zero error or change point is indicated with a dashed black line.

Comparison of both individual and averaged LEs/HEs and component derivatives across 9 transition metals (i.e., Sc-Cu) with CO, NH_3, and H_2O ligands (Table I) reveals several trends. For the carbonyl complexes, total-energy-derived EAs are largest, and the HEs and LEs are smallest at around -3 eV versus -3.4-3.5 eV for ammonia or -3.6-3.7 for water. Within the same ligand field, filling the 3*d* shell generally increases both the HE and LE. The DFT+U corrections to the total energy are on average small and negative (-0.04 eV/eV for CO, -0.10 eV/eV for NH_3 and -0.18 eV/eV for H_2O). Corrections of the *N*+1-electron HOMO are substantially steeper than those for the *N*-electron LUMO, averaging -0.3-0.4 eV/eV for the former versus 0.03-0.26 eV/eV for the latter.

Table I. Components of deviation from linearity in GGA results on octahedral complexes (in eV) as well as the dependence of those quantities on *U* (in eV/eV) and the point at which the curves become linear labeled 'Cross' (in eV). Maximum, minimum, and average values of select quantities are also tabulated.

CO

	HOMO Error	LUMO Error	ΔE	$\frac{\partial \varepsilon_{N+1}^{\mathrm{HOMO}}}{\partial U}$	$\frac{\partial \varepsilon_{N}^{\mathrm{LUMO}}}{\partial U}$	$\frac{\partial \Delta E}{\partial U}$	Cross
Sc	-2.77	-2.89	-16.57	-0.30	0.36	-0.03	8.1
Ti	-2.92	-2.91	-17.95	-0.30	0.35	0.01	9
V	-2.98	-2.99	-19.03	-0.34	0.42	0.02	7.7
Cr	-3.06	-3.02	-19.61	-0.12	-0.03	-0.07	100.9
Mn	-3.16	-3.03	-18.28	-0.20	-0.09	-0.14	95.1
Fe	-3.30	-3.25	-18.87	-0.46	0.45	-0.05	7.7
Co	-3.27	-3.15	-19.97	-0.44	0.40	-0.13	7.9
Ni	-3.25	-3.15	-21.23	-0.38	0.53	0.06	7.6
Cu	-2.98	-2.88	-19.04	-0.10	0.00	-0.04	93.9
min	-2.77	-2.88	-16.57	-0.10	-0.09	-0.14	
max	-3.30	-3.25	-21.23	-0.46	0.53	0.06	
avg	-3.07	-3.03	-18.95	-0.29	0.26	-0.04	

NH_3

	HOMO Error	LUMO Error	ΔE	$\frac{\partial \varepsilon_{N+1}^{\mathrm{HOMO}}}{\partial U}$	$\frac{\partial \varepsilon_{N}^{\mathrm{LUMO}}}{\partial U}$	$\frac{\partial \Delta E}{\partial U}$	Cross
Sc	-3.17	-3.45	-11.85	-0.40	0.32	-0.09	8.5
Ti	-3.56	-3.49	-13.03	-0.48	0.33	-0.10	9
V	-3.63	-3.55	-14.06	-0.49	0.36	-0.09	8.2
Cr	-3.35	-3.36	-12.34	-0.27	-0.06	-0.16	39.8
Mn	-3.43	-3.27	-14.16	-0.28	-0.10	-0.18	69.9
Fe	-3.85	-3.66	-14.51	-0.52	0.40	-0.09	7.9
Co	-3.74	-3.40	-15.72	-0.54	0.37	-0.07	8
Ni	-3.67	-3.42	-16.61	-0.55	0.53	-0.02	7.3
Cu	-3.09	-3.00	-15.08	-0.19	0.00	-0.08	45.1
min	-3.09	-3.00	-11.85	-0.19	-0.10	-0.18	
max	-3.85	-3.66	-16.61	-0.55	0.53	-0.02	
avg	-3.50	-3.40	-14.15	-0.41	0.24	-0.10	

H_2O

	HOMO Error	LUMO Error	ΔE	$\frac{\partial \varepsilon_{N+1}^{\mathrm{HOMO}}}{\partial U}$	$\frac{\partial \varepsilon_{N}^{\mathrm{LUMO}}}{\partial U}$	$\frac{\partial \Delta E}{\partial U}$	Cross
Sc	-3.16	-3.72	-12.33	-0.42	0.14	-0.15	12.2
Ti	-3.83	-3.75	-13.52	-0.46	0.16	-0.17	12.4
V	-3.97	-3.80	-14.68	-0.44	0.08	-0.19	14.10
Cr	-3.87	-3.86	-13.89	-0.33	-0.09	-0.22	35.7
Mn	-4.02	-3.81	-19.29	-0.35	-0.15	-0.23	52.3
Fe	-4.16	-3.71	-15.96	-0.54	0.11	-0.21	13.67
Co	-4.03	-3.70	-16.58	-0.45	0.11	-0.17	13.4
Ni	-3.32	-2.90	-18.13	-0.36	-0.05	-0.15	31.8
Cu	-3.48	-3.25	-17.51	-0.27	0.00	-0.12	38.6
min	-3.16	-2.90	-12.33	-0.27	-0.15	-0.23	
max	-4.16	-3.86	-19.29	-0.54	0.16	-0.12	

avg	-3.76	-3.61	-15.77	-0.40	0.03	-0.18

Recall from the theoretical model (see Sec. II), the LUMO must have a strong projection onto a fully unoccupied AO for the LUMO eigenvalue shift to be strongly positive with *U*. The LUMO shift is weaker because rehybridization of still occupied levels upon electron removal leads to some fractional occupation of the AO the likely diffuse LUMO projects onto. The LUMO error has the added disadvantage of interfering deconstructively with shifts in the total energy difference, meaning that only cases where an orbital is at least half emptied give rise to the desired behavior. In some cases, we do observe very efficient LUMO corrections with slopes around +0.53 eV/eV even in excess of the theoretical limit we predicted for a single orbital correction, due to occupations slightly above 1 (see supplementary material Table S2). As a practical note, the frontier orbital ordering may change at high *U*, and the appropriate orbital for use in the cubic spline may differ from the HOMO or LUMO (see example in supplementary material Figures S9-10). These results suggest that one can identify when DFT+U will be most effective at treating deviation from linearity errors without carrying out *E* vs. *q* calculations by identifying when the frontier MO energies are strongly *U* dependent, as evident from the occupation matrix itself or from finite difference of DFT and DFT+U eigenvalues.

DFT+U produces a linear energy profile at *U*=7-9 eV for six $M(CO)_6$ and $M(NH_3)_6$ complexes (M=Sc,Ti,V,Fe,Co,Ni) (complete details for all complexes are provided in supplementary material Tables S3-S30). This range of *U* values is within the realm of those applied in production DFT+U calculations, but inefficiencies are apparent for the hexa-aqua complexes and Cr, Mn, and Cu complexes regardless of ligand (see Sec. IV.C). For the hexa-aqua iron case, we added a *U* on O 2*p* states, which has seen some success[95], in order to bolster the standard DFT+U global curvature correction. This procedure worsened HOMO and LUMO

placement, increasing E^{dev} (see supplementary material Table S31). Intersite terms[96], found to be valuable for covalent metal-oxygen bonds[97], would not impact the weak metal-water interaction.

For comparison, we also studied the closed shell $Zn(H_2O)_6$, complex in which all 3*d* orbitals are filled and the HOMO and LUMO does not have strong 3*d* character. As expected from Sec. II, a "+U" correction has no effect on the global curvature (see supplementary material Table S32). DFT+U has been employed previously for d^{10} materials[98, 99], where special effort has been made to overcome the closed shell nature of the manifold in these cases for *U* calculation either by large potential shifts[100] or through HF calculations[101]. However, it is clear that d^{10} systems with no 3*d* character in frontier orbitals will have global curvatures that are immune to DFT+U.

C. Efficiency of "+U" corrections

We now examine observed DFT+U inefficiency in reducing GGA E^{dev} errors (Table I) with 1) reduced HE shifts for Mn, Cr, and Cu complexes and 2) broader small or incorrect-sign LE shifts. We quantify the effectiveness of DFT+U at reducing deviations from linearity by comparing the average GGA global curvature obtained from the difference in the *N*-electron LUMO and *N*+1-electron HOMO eigenvalues with the point at which a DFT+U correction produces straight-line energetics (Figure 7). The efficiency of DFT+U is thus defined as follows:

$$\text{Efficiency} = \frac{\left.\frac{\partial^2 E}{\partial q^2}\right|_{\text{GGA}}}{U_{\text{cross}}} \times 100 \ , \tag{29}$$

which is the percentage ratio of global curvature and the U_{cross} that produces linear *E* vs. *q*. The global curvature is highest for weak-field water ligands, with only $Ni(H_2O)_6$ as an exception, and lowest for strong-field carbonyl ligands, with ammonia generally residing between the two (Table II and Figure 7). The global curvature is generally largest for the middle of the periodic

table and smallest for nearly empty Sc (d^{0-1}) or nearly filled Cu (d^{8-9}) octahedral complexes. Efficiency, in turn, is highest overall for ammonia ligands and second for carbonyl ligands, with diminished efficiency on nearly all hexa-aqua complexes. This combined effect of lower efficiency but higher global curvature in hexa-aqua complexes means that not only would we project a high *U* needed between 7-8 eV from the GGA global curvature but that a *U* value closer to 14 eV would be required to achieve linearity once efficiency is taken into account. Such a large value of *U* is not typically practical to employ, and its necessity both in the water ligands and in select cases (i.e. Cr, Mn, and Cu) may be traced to being in the regime of incompletely filled and emptied occupations we previously identified in our theoretical model (see Sec. IV.D). Nevertheless, the high efficiencies (as much as 90-98%) for NH_3 and CO ligands suggest that DFT+U often succeeds in correcting both local and global curvature error as long as the numerical values of the two coincide strongly (see also Sec. IV.F).

Table II. Calculated *U* in eV for 2+ and 3+ octahedral complexes of metals (Sc-Cu) grouped by the relevant ligand (CO, NH_3, or H_2O) along with curvature (Curv., in eV), point of crossing (*U* labeled Cross, in eV), and efficiency (in %).

CO					
	U (2+)	*U* (3+)	Curv.	Cross	Efficiency
Sc	2.7	2.5	5.7	8.1	70%
Ti	4.8	4.4	5.8	9.0	65%
V	4.5	3.8	6.0	7.7	77%
Cr	3.4	3.0	6.0	101	6%
Mn	3.7	4.1	6.2	95	7%
Fe	4.3	3.9	6.5	7.7	85%
Co	6.9	5.0	6.4	7.9	81%
Ni	4.9	4.7	6.4	7.6	84%
Cu	8.6	8.2	5.9	94	6%
NH_3					
	U (2+)	*U* (3+)	Curv.	Cross	Efficiency
Sc	2.6	2.1	6.6	8.5	78%
Ti	4.1	3.9	7.0	9.0	78%
V	3.0	3.2	7.2	8.2	88%
Cr	2.0	2.7	6.7	40	17%
Mn	2.7	4.2	6.7	70	10%
Fe	3.3	3.7	7.5	7.9	95%

Co	4.1	4.7	7.1	8.0	90%
Ni	3.0	4.5	7.1	7.3	98%
Cu	6.1	7.1	6.1	45	14%
H_2O					
	U (2+)	*U* (3+)	Curv.	Cross	Efficiency
Sc	2.4	2.1	6.9	12.2	57%
Ti	3.8	3.6	7.6	12.4	61%
V	2.2	2.9	7.8	14.1	55%
Cr	1.6	2.2	7.7	36	22%
Mn	2.8	3.3	7.8	52	15%
Fe	2.9	4.1	7.9	13.7	58%
Co	4.0	4.7	7.7	13.4	58%
Ni	2.0	5.4	6.0	32	19%
Cu	5.7	7.5	6.7	39	17%

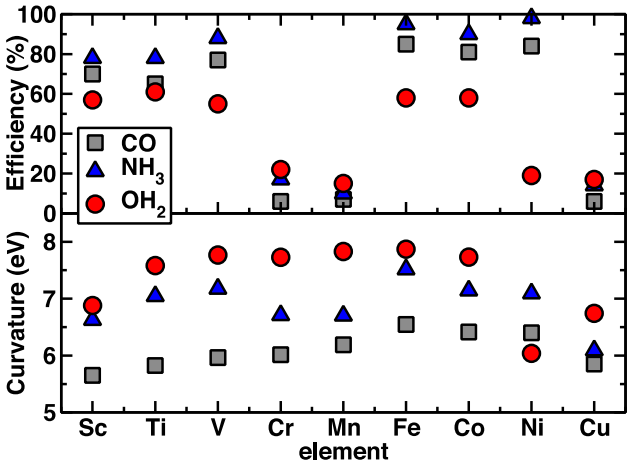

Figure 7. (Top) Efficiency of the DFT+U correction for octahedral transition metal complexes (M=Sc-Cu) with CO (gray squares), NH_3 (blue triangles), and OH_2 (red circles) ligands as measured by the expected *U* at which linearity occurs divided by the actual value of *U* required. (Bottom) Value of the curvature (in eV) obtained from +2 and +3 eigenvalues for the same complexes, which is the number employed as the expected *U* in the efficiency metric.

D. Occupation and density perspective on the "+U" correction

The behavior of DFT+U is derived from the occupation matrix properties, and we may interpret the efficiency and role of a "+U" correction on representative complexes through how the local occupation matrix changes as total charge, *q*, is varied. We revisit the example of $Mn(CO)_6$, which is a case where DFT+U is ineffective, and compare it to the non-pathological high-spin $Fe(CO)_6$ case (Figure 8). For Mn, a spin up orbital is only partially emptied as charge is varied, from *n*=1 at Mn(II) to about 0.75 at Mn(III), explaining the negative shift of the LUMO

with increasing U for Mn(III). From Mn(II) to Mn(III), spin down occupations increase, compensating the spin up occupation loss, leading to a negligible change in total on-site occupations (n_{tot}) across the range of q considered. The resulting fractionality increases weakly in an approximately linear fashion as a result of partial emptying of the spin up orbital. In the contrasting Fe case, a full (n=0.95) spin down orbital becomes nearly empty (n-Δn=0.04), and the fractionality peaks at around q=0.5 where the HOMO becomes half occupied. The total spin down 3d occupations only decrease from 1.5 to 1.0 as a result of rehybridization of other orbitals, but this compensation does not impact the fractionality.

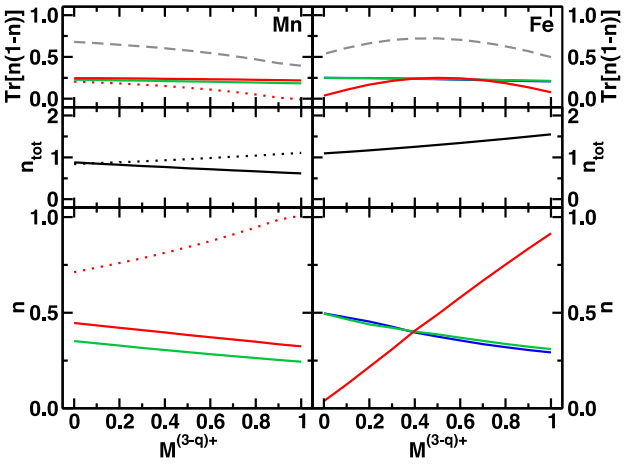

Figure 8. Comparison of features of $M(CO)_6$ metal d occupations in octahedral complexes with M=Mn (left) and M=Fe (right): (bottom) individual occupation matrix elements for spin up (dotted line) and spin down (dashed line), (middle) total occupations of the spin up (dotted) and down (solid) d electrons, and (top) total fractionality (gray dashed line) and contributing fractionality from individual states colored the same as in the bottom all as the total charge is varied from +3 to +2.

Within the other iron complexes, NH_3 ligands behave comparably to CO, with slightly more single projected AO emptying and enhanced fractionality at q = 0.5 (Figure 9). Conversely, the $Fe(H_2O)_6$ complex differs substantially: instead of the fully-occupied (i.e., all orbitals besides the HOMO), spin down AO occupation being split over two other orbitals, it is split over three orbitals, due to the weaker ligand field. In the other cases, the three occupied MOs are only the

t_{2g} orbitals, whereas the field is weak enough in the water case to include an e_g orbital. This altered occupation for the hexa-aqua complex gives an increase in fractionality as charge is depleted from +2 to +3, but these partial occupations increase from 0.0-0.2 for Fe(II) to around 0.25 in Fe(III). This splitting of occupations as charge is depleted toward Fe(III) results in a nearly monotonic increase in fractionality from Fe(II) to Fe(III), which we will show is what gives rise to inefficiency in a "+U" correction. Although the key AO corresponding to the frontier MO is nearly fully emptied to n-Δn=0.15, this value is higher than the other two iron complexes.

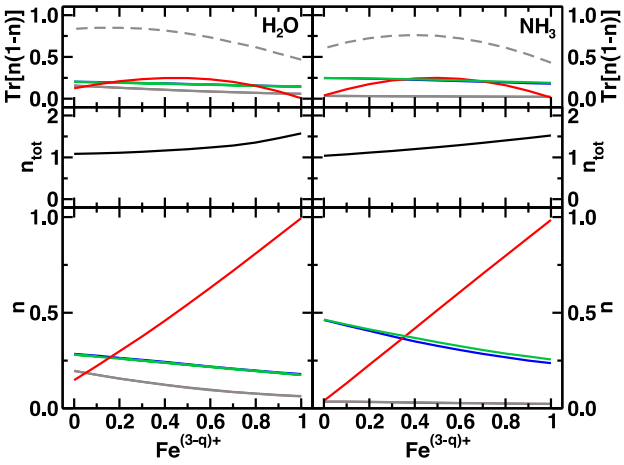

Figure 9. Comparison of features of spin down iron occupations in octahedral complexes with water (left) and ammonia (right) ligands: (bottom) individual occupation matrix elements, (middle) total occupations of the spin down *d* electrons, and (top) total fractionality (gray dashed line) and contributing fractionality from individual states colored the same as in the bottom all as the total charge is varied from +3 to +2.

Thus, we may summarize that from an occupation perspective in real systems what we previously identified in theoretical limits of the approach on idealized systems. DFT+U is ineffective at reducing deviations from linearity if: i) fractionality increases from one charge state to another due to reorganization of the occupations aside from the level being emptied or filled (e.g., the case of $Fe(H_2O)_6$) or ii) the state being emptied is only partially 3*d* orbital in

character and becomes only weakly emptied (e.g., the case of $Mn(CO)_6$).

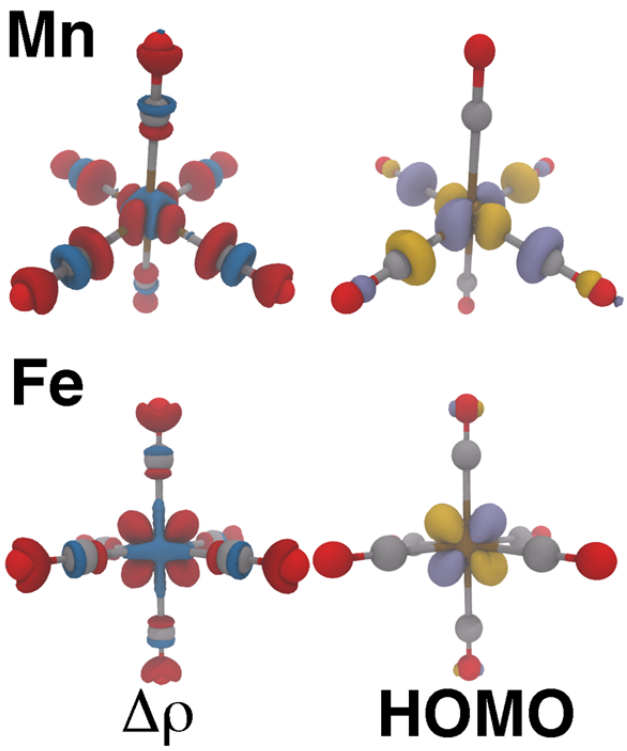

Figure 10. Density difference isosurface between the +2 and +3 states (left) and HOMO density (right) for $M(CO)_6$ complexes (M=Mn (top) and Fe (bottom)). The isosurfaces are colored as follows: (left) red represents an increase in density, blue represents a decrease as an electron is added and (right) yellow represents positive wavefunction phase and purple represents the negative wavefunction phase.

A comparison of the GGA *N*+1-electron HOMO density of the $Fe(CO)_6$ and $Mn(CO)_6$ molecules further reveals the reason that DFT+U is effective for correcting deviations from linearity of the former complex but not the latter. Although the $Fe(CO)_6$ HOMO is nearly exclusively centered on the metal center in a t_{2g}-like orbital expected from ligand field theory, the e_g $Mn(CO)_6$ molecular orbital has significant contribution from 2*p* states in the CO ligands (Figure 10). This combination in $Mn(CO)_6$ means that a projection of the MO onto AOs will produce intermediate occupations (see Figure 8) where DFT+U does very little to shift states up or down. It is important to note that by visual inspection, one might still describe the $Mn(CO)_6$ HOMO character as strongly atomic, as the majority of the density is localized on the Mn center.

However, even smaller contributions of electron density from the surrounding ligands limit the approach's effectiveness. The density difference ($\Delta\rho$) between the +2 and +3 states also reveals enhanced $\Delta\rho$ on the ligands for Mn versus more metal-centered density shifts in Fe (Figure 10). In total, the net percentage of density that is added directly to the metal center is 18% in the Mn case and 29% in the Fe case (see supplementary material). This density perspective suggests that a reformulation of the potential dependence on occupations is needed, e.g. to work directly with projecting maximally localized molecular orbitals onto the localized atomic-like orbital set or to a reformulation of the potential to address complex-wide delocalization error.

E. Fractionality as an indicator of efficiency in DFT+U corrections

Within the context of reducing E^{dev} errors with electron addition and removal, a motivating factor for employing DFT+U is that in the limit of a single atom with an orbital being emptied or filled, the fractionality should rise from zero at the endpoints to a maximum value of 0.25 when a ½ charge is added. In real systems, the fractionality of the endpoints is not zero, but a rise in fractionality may occur as fractional charge is added. Since we are interested in the correction to the curvature of the energy, we focus on the deviation of this fractionality (frac^{dev}) from a linear interpolation of the fractionality in the endpoints:

$$\text{frac}^{\text{dev}}(q) = \text{Tr}[\mathbf{n}_{N+q}(\mathbf{1}-\mathbf{n}_{N+q})] - q\,\text{Tr}[\mathbf{n}_{N+1}(\mathbf{1}-\mathbf{n}_{N+1})] - (1-q)\,\text{Tr}[\mathbf{n}_{N}(\mathbf{1}-\mathbf{n}_{N})], \qquad (30)$$

where the first term is the fractionality of the occupation matrix obtained with partial charge $N+q$ and the second and third terms are the linear average of the N+1- and N-electron fractionalities. We observe (Figure 11) that for cases where the DFT+U correction does nothing to alleviate global curvature errors, the fractionality appears linear over the range of charges considered and the frac^{dev} is near zero. Thus, these systems (e.g., $Cr(CO)_6$ and $Mn(CO)_6$ in Fig. 11) have a global curvature that is "invisible" to DFT+U because there is no increase in fractionality, even as the

total electron count is becoming more fractional. Instead, a "+U" energy correction will rigidly shift all points up equivalently, rather than selectively shifting up the points at fractional charge. This “invisibility” is a side-effect of employing the most common projection choice, i.e., atom-centered atomic basis functions. An alternate formulation of the definition of **n** that enters into the +U correction, e.g., the total electron count or in a molecular orbital basis for the projections, would recover corrections for these and other cases with comparable occupation matrix properties.

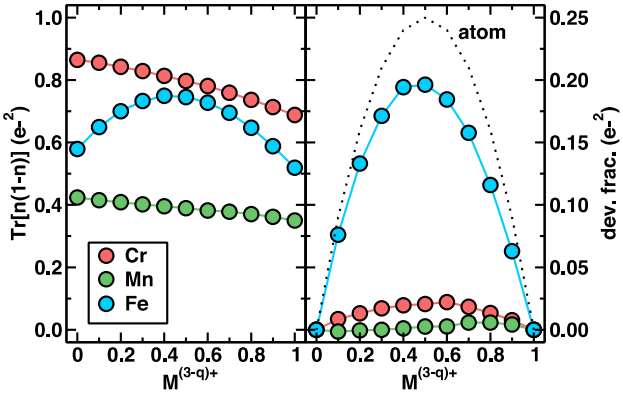

Figure 11. (Left) Fractionality (Tr[**n**(**1**-**n**)]) of $M(CO)_6$ (M=Cr, Mn, or Fe) as the charge on the complex is varied from +3 to +2 with symbols colored by element (Cr in salmon, Mn in green, Fe in blue). (Right) Deviation of fractionality (dev. frac.) from a linear admixture between M^{3+} and M^{2+} endpoints compared to the limiting case of an atom (black dotted line).

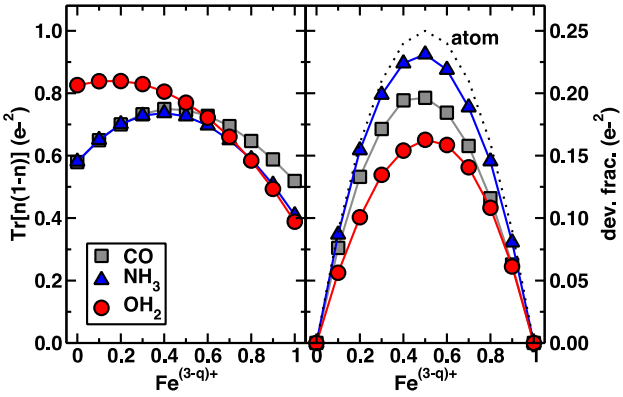

Figure 12. (Left) Fractionality (Tr[**n**(**1**-**n**)]) of $Fe(L)_6$ (L=CO, NH_3, or OH_2) as the charge on the complex is varied from +3 to +2 with symbols colored by ligand (gray squares for CO, blue

triangles for NH_3, and red circles for OH_2). (Right) Deviation of fractionality (dev. frac.) from a linear admixture between Fe^{3+} and Fe^{2+} endpoints compared to the limiting case of an atom (black dotted line).

We also revisit the fractionality and consider the $frac^{dev}$ for representative iron octahedral complexes with carbonyl, ammonia, and water ligands. For a strong ligand field, we expect that hybridization, and thus fractionality, would increase substantially over a weak field ligand. However, only in the Fe(II) endpoint is the fractionality of the carbonyl complex higher than the aqua complex (Figure 12). Instead, the weak field of the hexa-aqua complex gives rise to residual fractional occupations split over several states that peaks as charge is reduced toward Fe(III) (see Sec. IV.D). Because the Fe(III) endpoint of the hexa-aqua complex is close to the curve maximum, the $frac^{dev}$ is diminished. Ammonia fractionality is as low as water for Fe(II) but approaches lower fractionality that is comparable to CO at Fe(III). In contrast, NH_3 has low fractionality in both endpoints, which is comparable to H_2O at Fe(II) and CO at Fe(III), but peaks with fractionality comparable to CO at around +2.5. This behavior gives NH_3 the maximum $frac^{dev}$ of the three, which is nearly comparable to the limiting atom case (see Fig. 12). Thus, we can rationalize earlier efficiency observations: weak field ligands such as water may hybridize less and produce complexes with lower fractionality but weaker ligand fields may also increase fractionality via residual small amounts of minority spin *d* electron to be distributed equivalently over more AOs/MOs than in strong field cases.

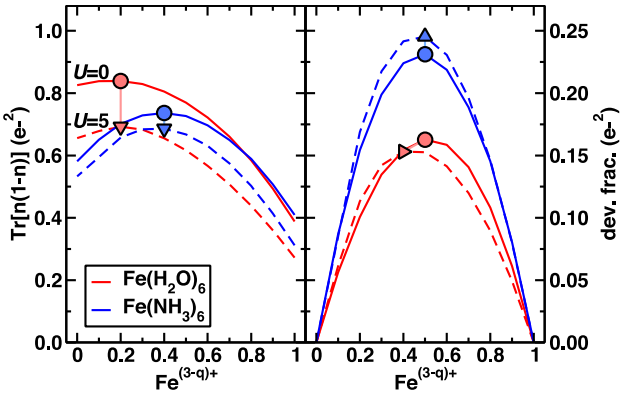

Figure 13. (Left) Fractionality (Tr[**n**(**1**-**n**)]) of $Fe(H_2O)_6$ in red and $Fe(NH_3)_6$ in blue as the charge on the complex is varied from +3 to +2 for GGA (solid line) and U = 5 eV (dashed line). The maximum of the GGA curve is indicated with a circle and a vector is drawn to the maximum on the U = 5 eV curve. (Right) Deviation of fractionality (dev. frac.) from a linear admixture between M^{3+} and M^{2+} endpoints for GGA (solid lines) and U = 5 eV (dashed lines) with the maximum of the GGA curve indicated with a circle and a vector is drawn to the maximum on the U = 5 eV curve.

Absolute fractionality at integer charge thus matters less than large $frac^{dev}$ increases at q=1/2 needed for DFT+U efficiency. The $frac^{dev}$ provides evidence of the extent to which a DFT+U correction will penalize the overstabilized GGA energies for fractional electron number and is proportional to the "+U" energy correction. Outside the low-U-limit approximation, DFT+U calculations with increasingly large U values applied should shift the fractionality by preferentially filling or emptying AOs/MOs (see Sec. II). Although one might expect all fractionality to be eliminated entirely, in practice (Figure 13), the shift is subtle. Namely, moving from GGA to a typically applied U value of 5 eV shifts absolute fractionalities by as much as 0.2 e^{-2}, about 25%. Interestingly, $Fe(H_2O)_6$ has a stronger decrease in fractionality with U than $Fe(NH_3)_6$ (Figure 13). However, the decrease in $Fe(H_2O)_6$ fractionality is distributed evenly across the curve, with the largest effect at the Fe(III) endpoint. When comparing the $Fe(H_2O)_6$ $frac^{dev}$ for U = 0 and 5 eV, $frac^{dev}$ is slightly reduced and its maximum is shifted off-center from q=+0.5. For $Fe(NH_3)_6$, on the other hand, the DFT+U reduction in fractionality is selectively effective on the endpoints by localizing the other MOs besides the Fe(II) HOMO/Fe(III) LUMO. This increases the $frac^{dev}$ even as overall fractionality decreases, amplifying the "+U" correction effectiveness as U increases, further explaining the relatively high efficiency of NH_3 complexes.

F. Global versus local curvature

Having observed that DFT+U can alleviate E^{dev} errors when a U that is at least as large as the initial GGA curvature is applied, one may be wondering do these E^{dev}-minimizing values of U bear any relation to linear response values of U? It is apparent that the practice[102] of choosing

a U value that adjusts the HOMO and LUMO to target positions or through IP-tuning commonly employed[33-42] in LRC hybrid functionals will directly alleviate deviations from linearity in the context of DFT+U as well. However, the U at which the HOMO and LUMO errors are corrected is sensitive to the nature of the projection scheme and not necessarily the same as the one obtained from linear response[103]. In order to address this outstanding question, we calculated the linear response U for all complexes in both the N+1 (M(II)) and N (M(III)) states (Table I) and investigate the relation of U to GGA global curvatures.

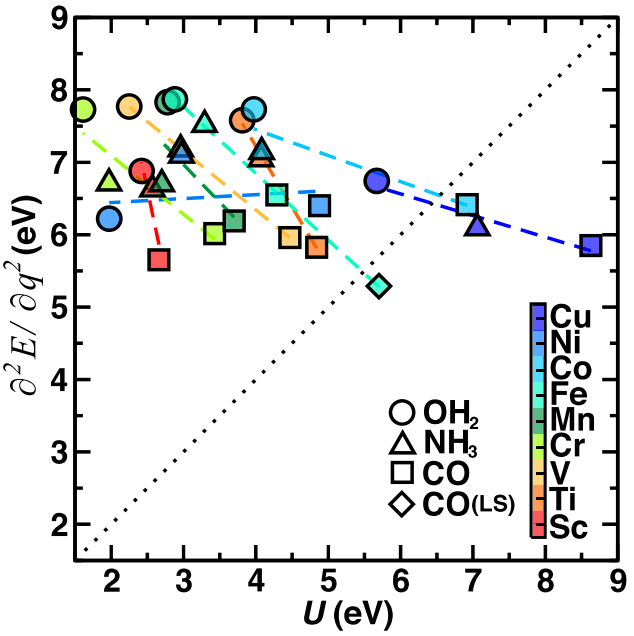

Figure 14. Plot of global curvature versus local curvature (U), both in eV, for the transition metals considered (from red Sc to blue Cu across the periodic table, as indicated by inset color bar) with y = x line shown in dotted black. Each symbol corresponds to a different ligand (circle OH_2, triangle NH_3, square CO and diamond for low-spin CO, as indicated in inset legend).

We first compare the U obtained for the N+1-electron state against the global curvature (Figure 14). The highest curvatures obtained for weak-field water ligands coincide to the lowest linear-response U values, and strong-field carbonyl ligands exhibit lower global curvatures and higher linear response U values across all complexes studied. Thus, there is an apparent negative

correlation between the ligand-field dependence of global curvature and linear response U. The only points where the two quantities appear to coincide are mid- to late-transition metals: Fe, Co and Cu, where the strongest field ligands have comparable linear response U and global curvature values. This result suggests that if one employs the linear response U value intending to simultaneously correct E^{dev}, e.g. for an octahedral hexa-aqua complex, then only a small percentage of the global curvature will be alleviated. This mismatch in global and local curvature (i.e. U) is further compounded by lower efficiencies for the weak field ligands (Table I).

The observed negative linear correlation between global and local curvature measures:

$$\frac{\partial^2 E}{\partial q^2} = mU + b \tag{31}$$

is quite strong with correlation coefficients (R^2) between 0.9 and 1.0, excluding only Mn and Ni (Table III). The slopes, m, are typically most negative for Sc and Ti, which are low d-occupation transition metals, and most other transition metals have slopes around -1 eV/eV of U. We consider the practical likelihood that the calculated linear response U would coincide with a value of U needed to correct E^{dev} at what we refer to as the equal curvature (EC) point. We note the average ($\bar{x}$) GGA curvature is 6.9 eV across the 27 molecules (range 5 to 8 eV) with a standard deviation (s) of 0.8 eV. The slope (m) and intercept (b) from the linear relationships obtained for each metal enable us to identify the EC point:

$$\text{EC} \equiv \frac{\partial^2 E}{\partial q^2} = U = \frac{b}{1-m} \ . \tag{32}$$

Next we determine the number of standard deviations (n_s) below $\bar{x}$ this predicted point would be, as the EC must occur when global curvature is low and linear response U is high:

$$n_s = \frac{\overline{x} - \mathrm{EC}}{s} \ . \tag{33}$$

With this analysis (Table III), the late transition metals Co, Ni, Cu have an EC point quite close to the average global curvature, whereas the EC is substantially below the average value for early transition metals (e.g. Sc-Mn). Next, we take into account the average efficiency (eff.) with which the DFT+U method corrects the global curvature for each metal with a modified expression for an effective equivalent curvature (EEC) point:

$$\mathrm{EEC} \equiv \frac{1}{\mathrm{eff.}} \frac{\partial^2 E}{\partial q^2} = U = \frac{b'}{1 - m'} \ . \tag{34}$$

The revised number of standard deviations, $n_{s,\mathrm{eff.}}$, that the crossing point is shifted off the mean increase once efficiency is taken into account in the EEC (Table III). It becomes clear that a linear response U would not eliminate E^{dev} especially for Sc, Cr, Mn, or Cu complexes, and the correspondence of linear response U and global curvature is likely best for the Fe, Co, and Ni systems to which DFT+U is widely applied[104-106] (Table III).

Table III. Summary of properties of lines relating global curvature and calculated U values including intercept (int.), slope, correlation coefficient (R^2), point where two curvatures are equal, standard deviations below average global curvature to satisfy point where two curvatures are equal(n_s), and the last two quantities repeated taking into account the average efficiency (eff.) of DFT+U for that metal.

	int.	slope	R^2	$\frac{\partial^2 E}{\partial q^2} = U$	n_s	$\frac{1}{\mathrm{eff.}} \frac{\partial^2 E}{\partial q^2} = U$	$n_{s,\mathrm{eff.}}$
Sc	18.5	-4.8	0.89	3.2	-4.4	2.5	-5.3
Ti	13.9	-1.7	1.00	5.2	-2.0	4.2	-3.3
V	9.6	-0.8	1.00	5.3	-1.9	4.8	-2.5
Cr	8.7	-0.8	0.90	4.8	-2.5	1.1	-7.0
Mn	10.1	-1.0	0.69	4.9	-2.3	0.7	-7.4
Fe	10.5	-0.9	1.00	5.5	-1.7	5.2	-2.0
Co	8.9	-0.4	0.91	6.5	-0.4	6.3	-0.8
Ni	6.3	0.1	0.15	6.7	-0.2	6.7	-0.2

Cu	8.4	-0.3	0.96	6.4	-0.6	2.1	-5.8

We also compared linear response *U* obtained at both integer (Table III) and fractional electron counts. Computing linear response *U* at +2 and +3 charge produces similar values for many of the compounds of interest typically within 0.5 eV of each other, although exceptions include cases where i) M(III) *U* values are in substantial excess of M(II) *U* values, e.g. $Ni(H_2O)_6$, $Mn(NH_3)_6$, and $Ni(NH_3)_6$ and ii) the reverse is true, e.g. $Co(CO)_6$. Overall, linear response *U* typically increases as the manifold is filled, regardless of ligand choice, and *U* values are smallest for the earliest transition metals, e.g. Sc, and for the Cr and Mn cases. There is limited correspondence between isoelectronic molecules, e.g. $Fe(III)(H_2O)_6$ versus $Mn(II)(H_2O)_6$, emphasizing our earlier observations[92] that *U* is sensitive to the underlying electronic structure.

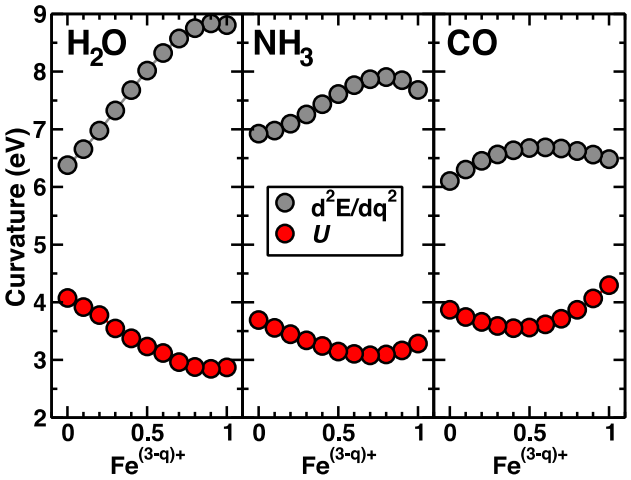

Figure 15. Measures of local (*U,* red circles) and global ($\frac{\partial^2 E}{\partial q^2}$, gray circles) curvature in eV for three octahedral iron complexes $Fe(L)_6$ with L=H_2O (left), NH_3 (middle), and CO (right) as the charge on the complex is varied from +3 to +2.

For the three high-spin $Fe(L)_6$ complexes with L=H_2O, NH_3, and CO, we computed global curvature and linear response *U* at fractional charges between the *N*+1- and *N*- electron integer values (Figure 15). In order to obtain global curvature at fractional charge, we fit the

fractional E vs. q curve to a fifth-order polynomial and took the second derivative to obtain $\left.\frac{\partial^2 E}{\partial q^2}\right|_q$. The result was not sensitive to the order of the fitting polynomial. We then evaluated linear response U at 0.1 increments of fractional total charge, which we believe is the first time such a calculation has been considered within plane-wave DFT+U. One argument in favor of the "+U" correction is its ability to exactly reproduce piecewise linearity and the derivative discontinuity in the atomic limit if a constant global curvature holds[70, 75]. Unlike CO and, to a lesser extent, NH_3 ligands, the computed global curvature data reveals variations that are especially strong for water ligands where the curvature ranges from 6 to 9 eV from Fe(III) to Fe(II), possibly motivating +U(q) correction in future work along the lines of the DFT+U(**R**) approach we have previously developed[107], where the U applied in this case is the global curvature at each q. As in DFT+U(**R**), DFT+U(q) total energies require only a reference point at which they are aligned for each value of U. In the +U(q) approach, a natural reference point is the higher-electron count charge state, and relative energies with U at each q may then be interpolated to obtain the precise E(q, U) at the appropriate global curvature value for that point. Within +U(q), one overcomes the lack of constant curvature (Figure 15), which may cause DFT+U E vs. q curves to be convex for some range of q and concave for other ranges. In fact, a demonstration of DFT+U(q) on $Fe(NH_3)_6$ reveals a nearly linear profile that cannot be achieved at constant applied U value (see supplementary material Figure S11).

In general, the Fe(III) species exhibits lower global curvature, which steadily increases towards the Fe(II) endpoint. The opposite trends are observed for linear response U as fractional charge is varied, and the two properties appear to be mirror images of each other, although no consistent correlation of the values across all values of q may be obtained. It may at first be counterintuitive that removing an electron from the transition metal center to another part of the

molecule versus removing it entirely (schematic in Figure 1) can lead to such different measures of energy curvature. However, we now present two arguments for why these global and local curvature measures should exhibit opposing trends.

First, consider the simplest case of an atom with n occupations and q charge. We will assume that the localized subshell of interest is emptied and filled when charge is varied (i.e., $\delta n = \delta q$), which is a good assumption for the frontier subshell in an open-shell atom. Recall that the local curvature or U ($\frac{\partial^2 E}{\partial n^2}$) and global curvature ($\frac{\partial^2 E}{\partial q^2}$) both may be defined in terms of two-point central difference formulae centered around the same point:

$$\frac{\partial^2 E}{\partial n^2} = \frac{E(n+\delta n)\big|_q - 2E(n)\big|_q + E(n-\delta n)\big|_q}{(\delta n)^2} \text{ and} \tag{35}$$

$$\frac{\partial^2 E}{\partial q^2} = \frac{E(n+\delta n)\big|_{q+\delta q} - 2E(n)\big|_q + E(n-\delta n)\big|_{q-\delta q}}{(\delta q)^2} \ , \tag{36}$$

where in the former, n is being varied directly, while in the latter n changes when q is varied. The two expressions will therefore be nontrivially equal if and only if:

$$E(n+\delta n)\big|_q + E(n-\delta n)\big|_q = E(n+\delta n)\big|_{q+\delta q} + E(n-\delta n)\big|_{q-\delta q} \ , \tag{37}$$

where the terms on the left-hand side represent the central difference terms from determination of the U obtained by varying onsite occupations at constant charge and the terms on the right-hand side represent the energies obtained by varying charge. We have no reason to expect these two quantities should be equal. To emphasize further, we may represent the same equality by returning the neutral term to represent these total energies instead as relative to the neutral case:

$$\Delta E(n+\delta n)\big|_q + \Delta E(n-\delta n)\big|_q = \Delta E(n+\delta n)\big|_{q+\delta q} + \Delta E(n-\delta n)\big|_{q-\delta q}\,, \tag{38}$$

where the Δ represents that each energy is a relative energy referenced against the $E(n)\big|_q$ value. At charge q, n is the occupation corresponding to the self-consistent stationary point, and adding or removing occupations from that manifold causes the energy to rise. Therefore, both terms on the left-hand side of eqn. 38 will be positive. On the right hand side, adding charge lowers the total energy, whereas removing charge makes the energy rise, giving one positive and one negative term. The extent to which those positive and negative terms do not cancel is what produces negative E^{dev} values. Therefore, it becomes clear that the global and local curvature measures are focused on two separate quantities and should only coincide out of chance.

A second argument pertains to the extent to which total energy errors at integer electrons are effectively reducing the computed global curvature. It has been observed[32, 57, 58, 61, 62] that curvature decreases as size increases in molecules. Here, we are studying molecules of comparable size but strong field ligands (e.g. CO) lead to higher effective hybridization than weak field ligands (e.g. H_2O). A comparison to Fe(II)/Fe(III) ions further highlights this effect as the global curvature decreases from its highest value at around 16 eV for Fe(II)/Fe(III) ions (see supplementary material Figures S12-13) to its smallest value in the low-spin $Fe(CO)_6$ complex of around 5 eV. The energies of inorganic complexes at integer electron count are artificially lowered through metal-ligand bond overdelocalization, whereas there is less opportunity for electrons to delocalize in an atom, producing lower computed curvatures as stronger ligands are added to a metal center. At the same time, linear response U targets exactly the opposite feature by answering: to what extent is hybridization at a constant charge overly favored within a molecule between states we expect to be localized? Therefore, when curvature decreases, we

would expect computed *U* to increase, as observed for several complexes (Figures 14 and 15).

The outcome of this study thus reinforces that if band-position-dependent properties are the main motivation for using DFT+U, then a *U* fit to reproduce key features of the density of states[102], or redefined as the value of *U* that eliminates HOMO-LUMO-derived definition of global curvature proposed by Stein et al.[32] (see eq. 2), is a better strategy than employing linear response *U*. Thankfully, for many of the materials to which DFT+U is most commonly employed, these two choices of *U* values often coincide quite closely (Table III). As a follow-up to this work, an ongoing area of interest for us is to identify how tuning delocalization error evidenced by convex energy behavior at non-integer occupations affects computed endpoint properties such as spin state ordering.

V. CONCLUSIONS

We have developed understanding of where DFT+U, a method designed to treat unphysical local curvature that governs delocalization between atomic subshells and surrounding atoms in molecules and solids, is suitable for simultaneously treating global curvature errors indicated by deviations from linearity in energy with electron removal or addition. We have provided quantitative criteria for DFT+U efficiency in correcting deviations from linearity: i) strong AO character in the HOMO and LUMO and ii) strong loss of the AO character from the MO as the MO is emptied without reorganization of that character into other occupied states. We have determined that under no circumstances should DFT+U with positive *U* values increase convex deviations from linearity. We have identified the maximum efficiency of DFT+U to correct curvature as -0.125 eV/eV of *U*, which corresponds to moderate *U* values around 5-6 eV for only a select subset of mid- to late-transition metal complexes with strong field ligands, which are coincidentally among the complexes most typically studied with this method. We demonstrated additional requirements for efficiency including that the occupations must show

deviations from linearity at fractional charge for the method to identify delocalization error. This criterion is not satisfied in Mn and Cr complexes that therefore remain uncorrected by DFT+U. Similar logic applies to no reduction in deviation from linearity in closed shell complexes.

Finally, we provided a firm case and quantitative evidence that local and global curvature measures on a complex should not coincide. We observed that increasing ligand field strength increases the effective size of the complex for the delocalizing 3*d* electrons in the frontier orbitals, leading to reduced curvature. Conversely, strong field ligands increase the measure of on-site unphysical curvature. We identified late transition metals with strong field ligands as the rare cases in which the two quantities would coincide. Indeed, based on typical practices in the literature, correcting DFT+U to alleviate local curvature likely leaves behind residual global curvature. This work highlights the need to develop an understanding of when employing tuning strategies for alleviating global energetic deviations from linearity improves or worsens density-delocalization driven total-energy errors at integer electron count.

SUPPLEMENTARY MATERIAL

See supplementary material for optimized geometries, list of pseudopotentials used, calculated and interpolated deviations from linearity for eight octahedral complexes, eigenvalue crossing analysis and interpolation, and complete components of interpolation for 28 octahedral complexes, interpolation and calculated results on an iron atom, results with U on O 2p, example occupations, method for density difference calculation, and demonstration of a DFT+U(q) approach.

ACKNOWLEDGMENTS

This work was supported by a Reed grant from the MIT Research Support Corporation and an MIT Energy Initiative Seed Grant. The authors acknowledge partial support by the National Science Foundation under grant number ECCS-1449291. H.J.K. holds a Career Award at the

Scientific Interface from the Burroughs Wellcome Fund. The authors thank Adam H. Steeves for providing a critical reading of the manuscript.

APPENDIX: CALCULATING *U*

By exploiting Janak's theorem[30] in DFT, U may instead be calculated in terms of eigenvalue differences:

$$U = \varepsilon^I_{nl,m_l}(n^I_{nl} + \frac{1}{2}) - \varepsilon^I_{nl,m_l}(n^I_{nl} - \frac{1}{2}) \,, \tag{A39}$$

which is the finite difference expression of:

$$U = \frac{\partial \varepsilon^I_{nl,m_l}}{\partial n^I_{nl}} \,. \tag{A40}$$

Within linear response U[75], rather than directly constraining occupations, a linear shift is applied to the localized occupations:

$$E^{\text{lin}} = \sum_{I,\sigma} \sum_{nl} \alpha^I_{nl} \text{Tr}(\mathbf{n}^{I,\sigma}_{nl}) \,, \tag{A41}$$

where α^I_{nl} is only applied to the *nl* subshell of atom *I*. This rigid potential shift adjusts the eigenvalues of MOs with strong projection onto the AO subshell of interest as:

$$V^{\text{lin}} = \sum_{I,nl} \sum_{m} \alpha^I_{nl} \left| \phi^I_{nl,m} \right\rangle \left\langle \phi^I_{nl,m} \right| \,, \tag{A42}$$

where this correction is additive with any underlying xc approximation potential and the "+U" potential shift in eqn. 11 if they are simultaneously applied. As the potential shift moves MOs

with strong *nl* subshell character, it alters the filling of the AOs that the MOs project onto, leading to reorganization of the occupations. This procedure was first introduced by Pickett and coworkers[91] and later clarified by Cococcioni and de Gironcoli[75] to remove any non-interacting or 'bare' shift in occupations that would occur as a result of the shift in level positions. In practice, U is computed by inverting the slope of the line obtained by applying several values of α against the bare and converged total occupations of the subshell of interest as follows:

$$U_{nl}^{I} = \frac{d\alpha_{nl}^{I}}{d(n_{nl}^{I})_0} - \frac{d\alpha_{nl}^{I}}{dn_{nl}^{I}} , \tag{A43}$$

where the first term represents the bare contribution that is removed from the converged solution. A self-consistent extension[77] to this original approach enabled the calculation of U directly on the DFT+U density as follows:

$$U_{\text{out}} = U_{\text{scf}} - U_{\text{in}} / m , \tag{A44}$$

where m is a degeneracy factor and U_{scf} is obtained by applying several values of U_{in}, computing U_{out}, and extrapolating back to the U_{in}=0 limit. This approach is motivated when the standard xc approximation and DFT+U electronic states differ substantially. More recently, it has been shown[70] that freezing the U potential during the linear response calculation may equivalently be used to obtain the U from a DFT+U density. Alternatively, one can return to the original expression of U (eqn. 3) and simply obtain the energy contribution from the underlying xc approximation in the DFT+U calculation and fit to a quadratic form against the total occupations.

REFERENCES

1. A. Jain, S. P. Ong, G. Hautier, W. Chen, W. D. Richards, S. Dacek, S. Cholia, D. Gunter, D. Skinner, and G. Ceder, APL Materials **1**, 011002 (2013).
2. J. K. Nørskov, and T. Bligaard, Angewandte Chemie International Edition **52**, 776 (2013).

3. P. Mori-Sánchez, A. J. Cohen, and W. Yang, J. Chem. Phys. **125**, 201102 (2006).
4. A. Ruzsinszky, J. P. Perdew, G. I. Csonka, O. A. Vydrov, and G. E. Scuseria, J. Chem. Phys. **126**, 104102 (2007).
5. R. Haunschild, T. M. Henderson, C. A. Jiménez-Hoyos, and G. E. Scuseria, J. Chem. Phys. **133**, 134116 (2010).
6. A. J. Cohen, P. Mori-Sánchez, and W. Yang, Science **321**, 792 (2008).
7. T. Schmidt, and S. Kümmel, Phys. Rev. B **93**, 165120 (2016).
8. A. Ruzsinszky, J. P. Perdew, G. I. Csonka, O. A. Vydrov, and G. E. Scuseria, J. Chem. Phys. **125**, 194112 (2006).
9. A. D. Dutoi, and M. Head-Gordon, Chem. Phys. Lett. **422**, 230 (2006).
10. T. Bally, and G. N. Sastry, J. Phys. Chem. A **101**, 7923 (1997).
11. Y. Zhang, and W. Yang, J. Chem. Phys. **109**, 2604 (1998).
12. B. G. Johnson, C. A. Gonzales, P. M. W. Gill, and J. A. Pople, Chem. Phys. Lett. **221**, 100 (1994).
13. P. Mori-Sánchez, A. J. Cohen, and W. Yang, Phys. Rev. Lett. **100**, 146401 (2008).
14. A. J. Cohen, P. Mori-Sánchez, and W. Yang, Phys. Rev. B **77**, 115123 (2008).
15. D. J. Tozer, and F. De Proft, J. Phys. Chem. A **109**, 8923 (2005).
16. A. M. Teale, F. De Proft, and D. J. Tozer, J. Chem. Phys. **129**, 044110 (2008).
17. M. J. G. Peach, A. M. Teale, T. Helgaker, and D. J. Tozer, J. Chem. Theory Comput. **11**, 5262 (2015).
18. M.-C. Kim, E. Sim, and K. Burke, Phys. Rev. Lett. **111**, 073003 (2013).
19. X. Zheng, M. Liu, E. R. Johnson, J. Contreras-García, and W. Yang, J. Chem. Phys. **137**, 214106 (2012).
20. E. R. Johnson, A. Otero-de-la-Roza, and S. G. Dale, J. Chem. Phys. **139**, 184116 (2013).
21. J. P. Perdew, R. G. Parr, M. Levy, and J. L. Balduz, Phys. Rev. Lett. **49**, 1691 (1982).
22. W. Yang, Y. Zhang, and P. W. Ayers, Phys. Rev. Lett. **84**, 5172 (2000).
23. J. P. Perdew, and M. Levy, Phys. Rev. Lett. **51**, 1884 (1983).
24. L. J. Sham, and M. Schlüter, Phys. Rev. Lett. **51**, 1888 (1983).
25. E. Sagvolden, and J. P. Perdew, Phys. Rev. A **77**, 012517 (2008).
26. P. Mori-Sanchez, and A. J. Cohen, Phys. Chem. Chem. Phys. **16**, 14378 (2014).
27. E. Kraisler, and L. Kronik, J. Chem. Phys. **140**, 18A540 (2014).
28. G. K.-L. Chan, J. Chem. Phys. **110**, 4710 (1999).
29. O. A. Vydrov, G. E. Scuseria, and J. P. Perdew, J. Chem. Phys. **126**, 154109 (2007).
30. J. F. Janak, Phys. Rev. B **18**, 7165 (1978).
31. T. Koopmans, Physica **1**, 104 (1934).
32. T. Stein, J. Autschbach, N. Govind, L. Kronik, and R. Baer, J. Phys. Chem. Lett. **3**, 3740 (2012).
33. E. Livshits, and R. Baer, Phys. Chem. Chem. Phys. **9**, 2932 (2007).
34. L. Kronik, T. Stein, S. Refaely-Abramson, and R. Baer, J. Chem. Theory Comput. **8**, 1515 (2012).
35. T. Stein, L. Kronik, and R. Baer, J. Am. Chem. Soc. **131**, 2818 (2009).
36. T. Stein, L. Kronik, and R. Baer, J. Chem. Phys. **131**, 244119 (2009).
37. M. Srebro, and J. Autschbach, J. Phys. Chem. Lett. **3**, 576 (2012).
38. T. Körzdörfer, and J.-L. Brédas, Acc. Chem. Res. **47**, 3284 (2014).
39. J. Autschbach, and M. Srebro, Acc. Chem. Res. **47**, 2592 (2014).
40. J. D. Gledhill, M. J. G. Peach, and D. J. Tozer, J. Chem. Theory Comput. **9**, 4414 (2013).

41. T. Stein, H. Eisenberg, L. Kronik, and R. Baer, Phys. Rev. Lett. **105**, 266802 (2010).
42. U. Salzner, and R. Baer, J. Chem. Phys. **131**, 231101 (2009).
43. T. Leininger, H. Stoll, H.-J. Werner, and A. Savin, Chem. Phys. Lett. **275**, 151 (1997).
44. J. Toulouse, F. Colonna, and A. Savin, Phys. Rev. A **70**, 062505 (2004).
45. O. A. Vydrov, and G. E. Scuseria, J. Chem. Phys. **125**, 234109 (2006).
46. A. J. Cohen, P. Mori-Sánchez, and W. Yang, J. Chem. Phys. **126**, 191109 (2007).
47. H. Iikura, T. Tsuneda, T. Yanai, and K. Hirao, J. Chem. Phys. **115**, 3540 (2001).
48. R. Baer, and D. Neuhauser, Phys. Rev. Lett. **94**, 043002 (2005).
49. T. Tsuneda, J.-W. Song, S. Suzuki, and K. Hirao, J. Chem. Phys. **133**, 174101 (2010).
50. S. Refaely-Abramson, R. Baer, and L. Kronik, Phys. Rev. B **84**, 075144 (2011).
51. T. Heaton-Burgess, and W. Yang, J. Chem. Phys. **132**, 234113 (2010).
52. H. Sun, and J. Autschbach, ChemPhysChem **14**, 2450 (2013).
53. J. D. Gledhill, and D. J. Tozer, J. Chem. Phys. **143**, 024104 (2015).
54. T. Schmidt, E. Kraisler, A. Makmal, L. Kronik, and S. Kümmel, J. Chem. Phys. **140**, 18A510 (2014).
55. C. Li, X. Zheng, A. J. Cohen, P. Mori-Sánchez, and W. Yang, Phys. Rev. Lett. **114**, 053001 (2015).
56. M. Dauth, F. Caruso, S. Kümmel, and P. Rinke, Phys. Rev. B **93**, 121115 (2016).
57. A. Karolewski, L. Kronik, and S. Kümmel, J. Chem. Phys. **138**, 204115 (2013).
58. S. R. Whittleton, X. A. Sosa Vazquez, C. M. Isborn, and E. R. Johnson, J. Chem. Phys. **142**, 184106 (2015).
59. T. Körzdörfer, R. M. Parrish, J. S. Sears, C. D. Sherrill, and J.-L. Brédas, J. Chem. Phys. **137**, 124305 (2012).
60. K. Garrett, X. Sosa Vazquez, S. B. Egri, J. Wilmer, L. E. Johnson, B. H. Robinson, and C. M. Isborn, J. Chem. Theory Comput. **10**, 3821 (2014).
61. T. Körzdörfer, J. S. Sears, C. Sutton, and J.-L. Brédas, J. Chem. Phys. **135**, 204107 (2011).
62. V. Vlček, H. R. Eisenberg, G. Steinle-Neumann, L. Kronik, and R. Baer, J. Chem. Phys. **142**, 034107 (2015).
63. J. P. Perdew, and A. Zunger, Phys. Rev. B **23**, 5048 (1981).
64. A. Filippetti, and N. A. Spaldin, Phys. Rev. B **67**, 125109 (2003).
65. I. Dabo, A. Ferretti, N. Poilvert, Y. Li, N. Marzari, and M. Cococcioni, Phys. Rev. B **82**, 115121 (2010).
66. M. R. Pederson, A. Ruzsinszky, and J. P. Perdew, J. Chem. Phys. **140**, 121103 (2014).
67. J. P. Perdew, A. Ruzsinszky, J. Sun, and M. R. Pederson, Advances In Atomic, Molecular, and Optical Physics **64**, 1 (2015).
68. M. R. Pederson, T. Baruah, D.-y. Kao, and L. Basurto, J. Chem. Phys. **144**, 164117 (2016).
69. V. Anisimov, I. Solovyev, M. Korotin, M. Czyżyk, and G. Sawatzky, Phys. Rev. B **48**, 16929 (1993).
70. B. Himmetoglu, A. Floris, S. Gironcoli, and M. Cococcioni, Int. J. Quantum Chem. **114**, 14 (2014).
71. V. I. Anisimov, and O. Gunnarsson, Phys. Rev. B **43**, 7570 (1991).
72. V. I. Anisimov, J. Zaanen, and O. K. Andersen, Phys. Rev. B **44**, 943 (1991).
73. A. I. Liechtenstein, V. I. Anisimov, and J. Zaanen, Phys. Rev. B **52**, R5467 (1995).
74. V. I. Anisimov, F. Aryasetiawan, and A. I. Lichtenstein, J. Phys.: Condens. Matter **9**, 767 (1997).
75. M. Cococcioni, and S. de Gironcoli, Phys. Rev. B **71** (2005).

76. S. L. Dudarev, G. A. Botton, S. Y. Savrasov, C. J. Humphreys, and A. P. Sutton, Phys. Rev. B **57**, 1505 (1998).
77. H. J. Kulik, M. Cococcioni, D. A. Scherlis, and N. Marzari, Physical Review Letters **97**, 103001 (2006).
78. H. J. Kulik, N. Seelam, B. Mar, and T. J. Martinez, Journal of Physical Chemistry A **just accepted** (2016).
79. H. J. Kulik, The Journal of Chemical Physics **142**, 240901 (2015).
80. P. Giannozzi, S. Baroni, N. Bonini, M. Calandra, R. Car, C. Cavazzoni, D. Ceresoli, G. L. Chiarotti, M. Cococcioni, and I. Dabo, J. Phys.: Condens. Matter **21**, 395502 (2009).
81. J. P. Perdew, K. Burke, and M. Ernzerhof, Phys. Rev. Lett. **77**, 3865 (1996).
82. D. Vanderbilt, Phys. Rev. B **41**, 7892 (1990).
83. A. M. Derfus, W. C. W. Chan, and S. N. Bhatia, Nano Letters **4**, 11 (2004).
84. A. M. Rappe, K. M. Rabe, E. Kaxiras, and J. Joannopoulos, Phys. Rev. B **41**, 1227 (1990).
85. G. J. Martyna, and M. E. Tuckerman, J. Chem. Phys. **110**, 2810 (1999).
86. E. I. Ioannidis, T. Z. H. Gani, and H. J. Kulik, Journal of Computational Chemistry, n/a (2016).
87. A. Kramida, Ralchenko, Yu., Reader, J. and NIST ASD Team, NIST Atomic Spectra Database (version 5.3), [Online]. (2015).
88. E. I. Ioannidis, and H. J. Kulik, The Journal of Chemical Physics **143**, 034104 (2015).
89. S. R. Mortensen, and K. P. Kepp, J. Phys. Chem. A (2015).
90. S. J. Lippard, and J. M. Berg, *Principles of bioinorganic chemistry* (University Science Books, 1994).
91. W. E. Pickett, S. C. Erwin, and E. C. Ethridge, Phys. Rev. B **58**, 1201 (1998).
92. H. J. Kulik, and N. Marzari, Journal of Chemical Physics **133**, 114103 (2010).
93. B. Meredig, A. Thompson, H. A. Hansen, C. Wolverton, and A. van de Walle, Phys. Rev. B **82** (2010).
94. H. J. Kulik, and N. Marzari, Journal of Chemical Physics **129**, 134314 (2008).
95. L. Jiang, S. Levchenko, and A. Rappe, Phys. Rev. Lett. **108**, 166403 (2012).
96. V. L. Campo, Jr., and M. Cococcioni, J. Phys.: Condens. Matter **22** (2010).
97. H. J. Kulik, and N. Marzari, Journal of Chemical Physics **134**, 094103 (2011).
98. K. Yu, and E. A. Carter, J. Chem. Phys. **140**, 121105 (2014).
99. S.-j. Hu, S.-s. Yan, M.-w. Zhao, and L.-m. Mei, Phys. Rev. B **73**, 245205 (2006).
100. W.-J. Lee, and Y.-S. Kim, J. Korean Phys. Soc. **60**, 781 (2012).
101. N. J. Mosey, and E. A. Carter, Phys. Rev. B **76**, 155123 (2007).
102. C. Loschen, J. Carrasco, K. M. Neyman, and F. Illas, Phys. Rev. B **75**, 035115 (2007).
103. D. D. O'Regan, N. D. Hine, M. C. Payne, and A. A. Mostofi, Phys. Rev. B **82**, 081102 (2010).
104. P. Vassilaras, A. J. Toumar, and G. Ceder, Electrochem. Commun. **38**, 79 (2014).
105. D. Friebel, M. W. Louie, M. Bajdich, K. E. Sanwald, Y. Cai, A. M. Wise, M.-J. Cheng, D. Sokaras, T.-C. Weng, and R. Alonso-Mori, J. Am. Chem. Soc. **137**, 1305 (2015).
106. D. Santos-Carballal, A. Roldan, R. Grau-Crespo, and N. H. de Leeuw, Phys. Rev. B **91**, 195106 (2015).
107. H. J. Kulik, and N. Marzari, Journal of Chemical Physics **135**, 194105 (2011).

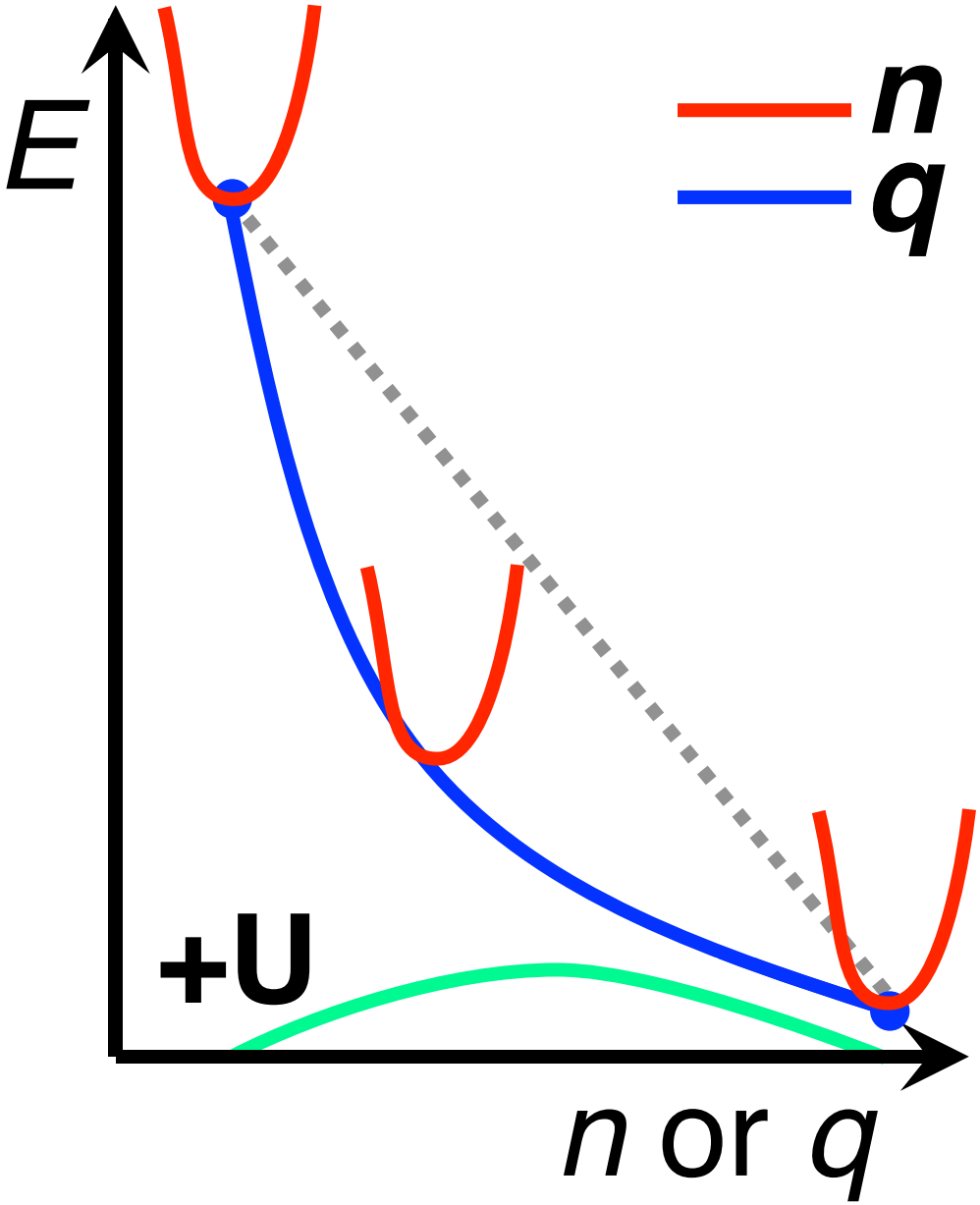

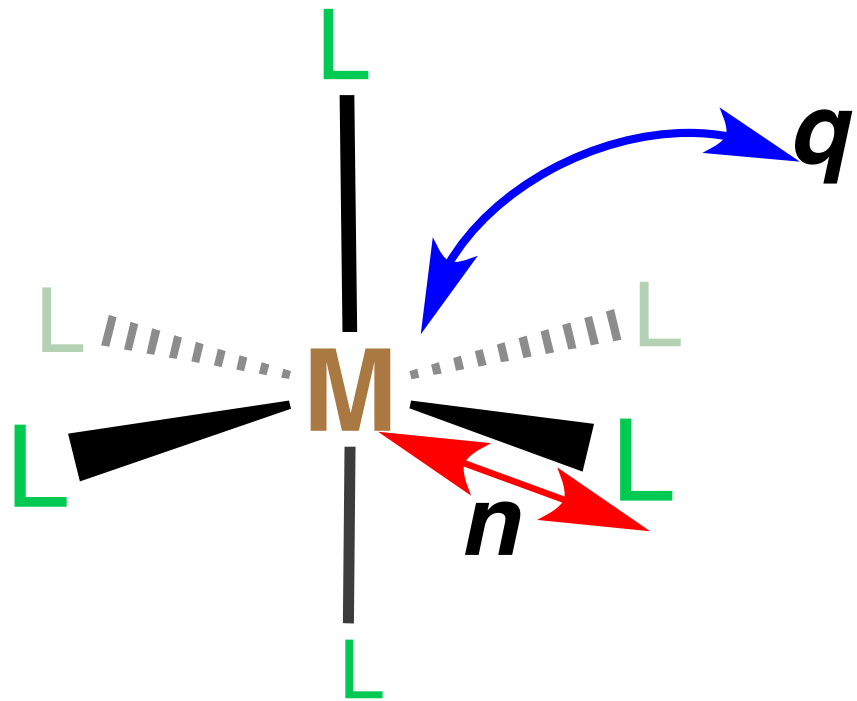

M=Sc-Cu

L=CO,NH_3,H_2O

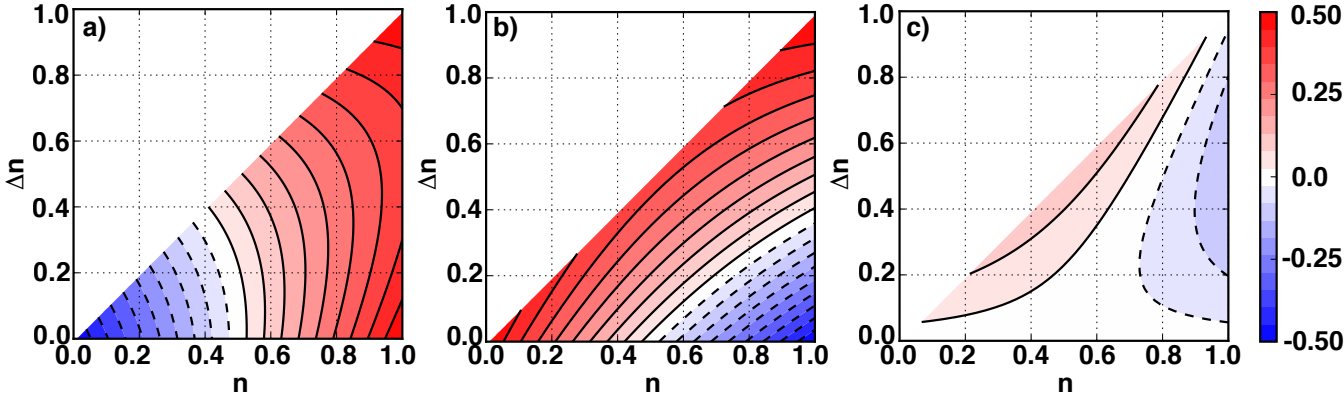
a)
b)
c)
Δn
n
0.0
0.2
0.4
0.6
0.8
1.0
0.50
0.25
0.0
-0.25
-0.50

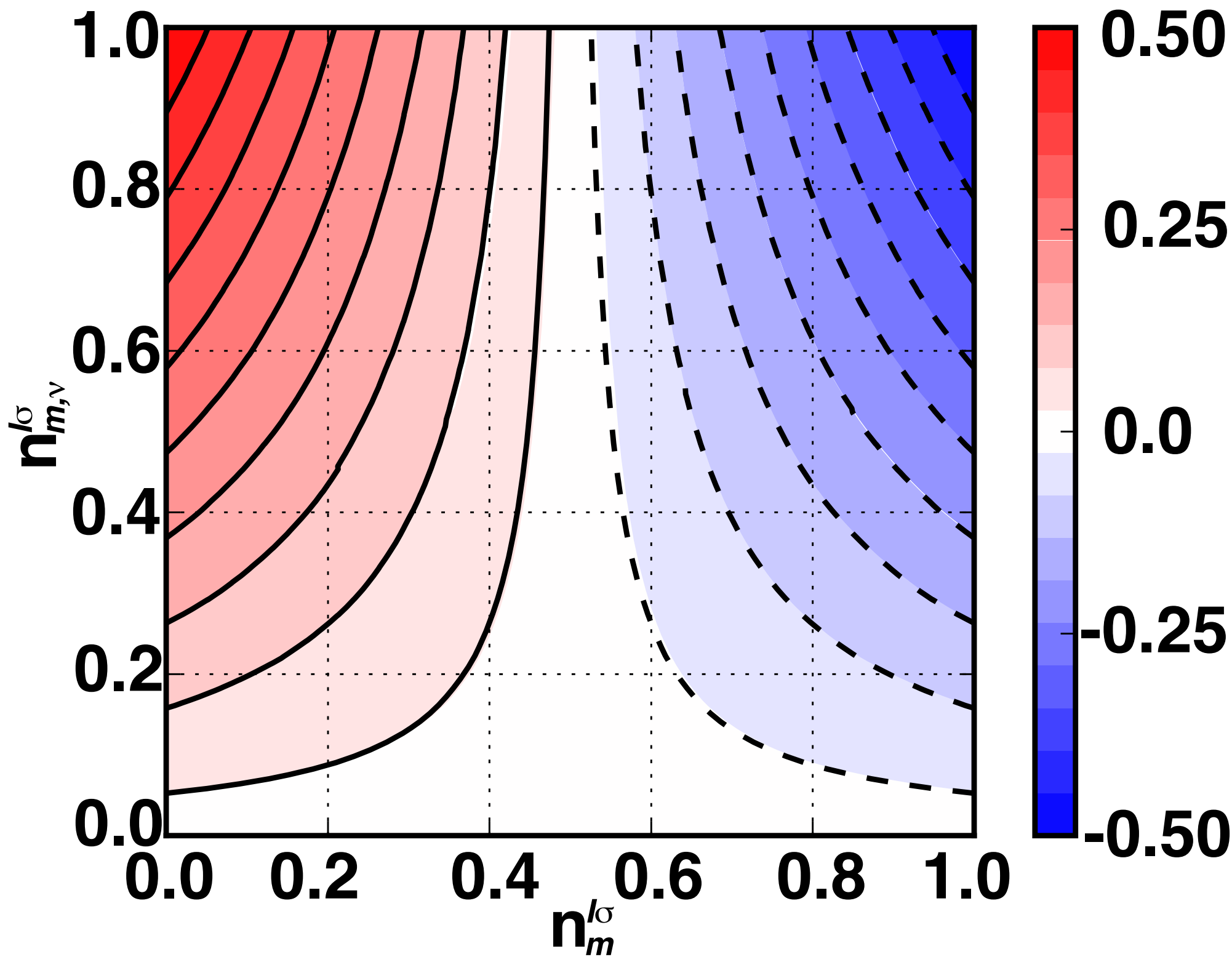
1.0
0.8
0.6
0.4
0.2
0.0
$n^{l\sigma}_{m,\nu}$
0.0
0.2
0.4
0.6
0.8
1.0
$n^{l\sigma}_{m}$
0.50
0.25
0.0
-0.25
-0.50

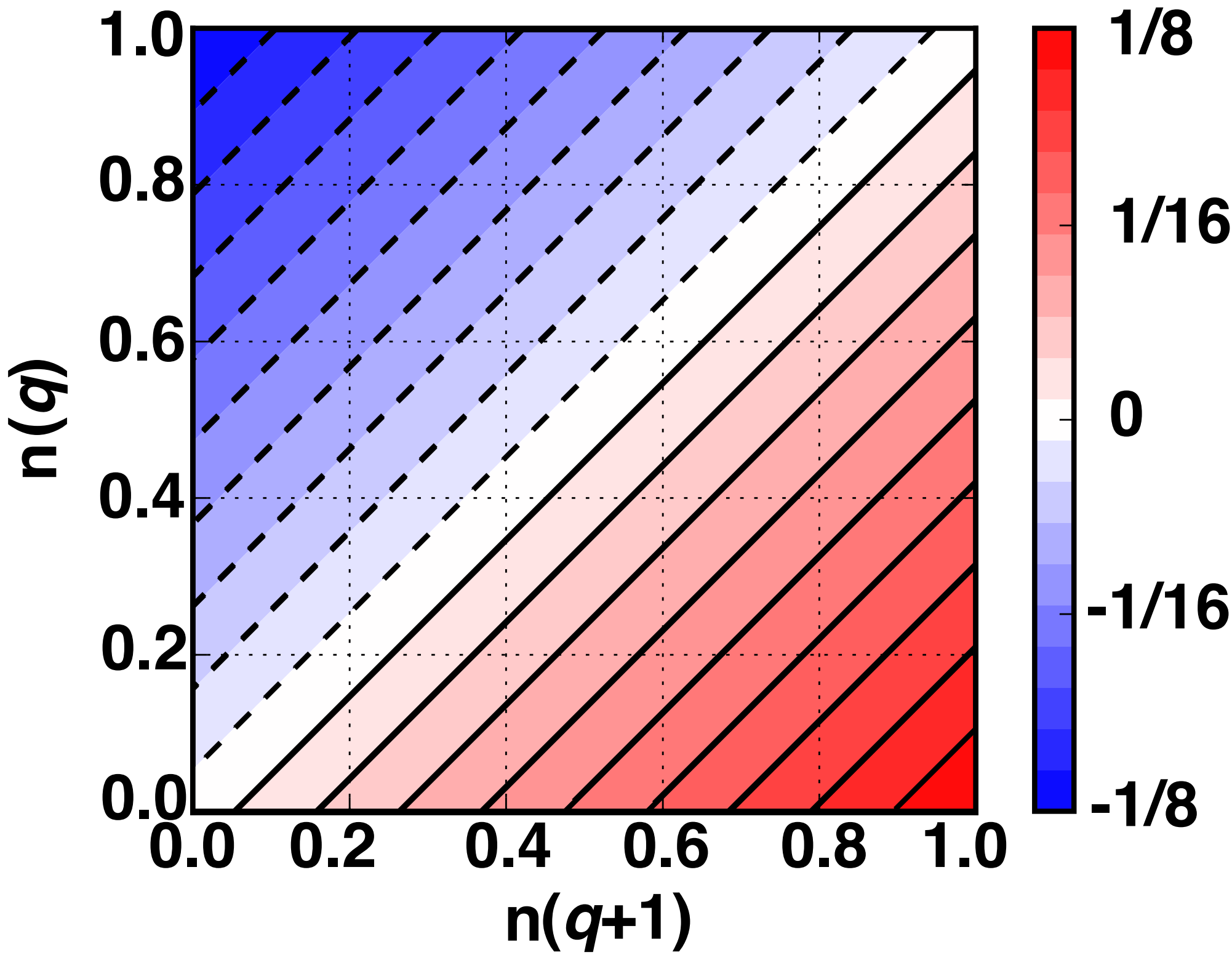
1.0
0.8
0.6
0.4
0.2
0.0
n(q)
0.0
0.2
0.4
0.6
0.8
1.0
n(q+1)
1/8
1/16
0
-1/16
-1/8

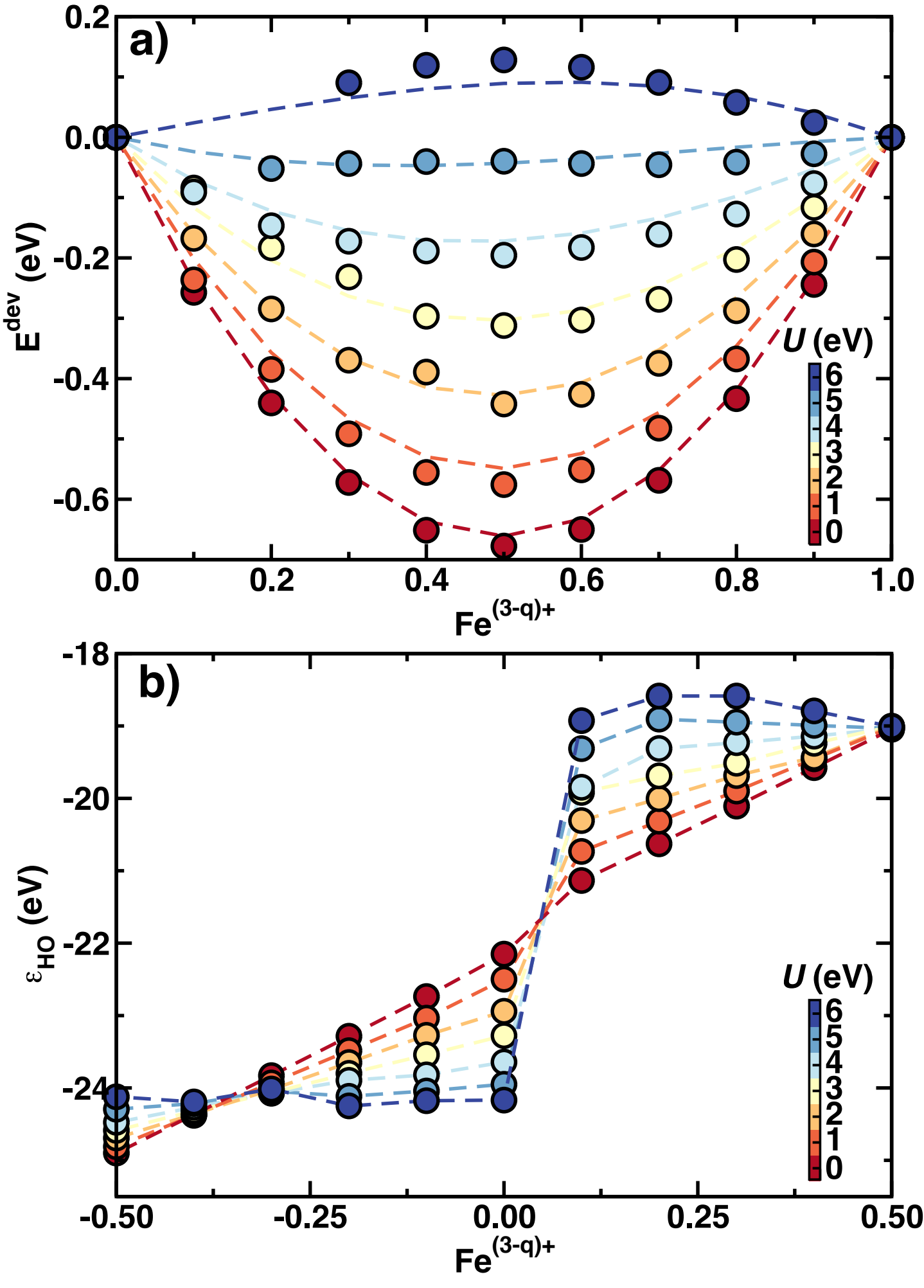
a)
0.2
0.0
-0.2
-0.4
-0.6
E^{dev} (eV)
0.0
0.2
0.4
0.6
0.8
1.0
$Fe^{(3-q)+}$
U (eV)
6
5
4
3
2
1
0
b)
-18
-20
-22
-24
ε_{HO} (eV)
-0.50
-0.25
0.00
0.25
0.50
$Fe^{(3-q)+}$
U (eV)
6
5
4
3
2
1
0

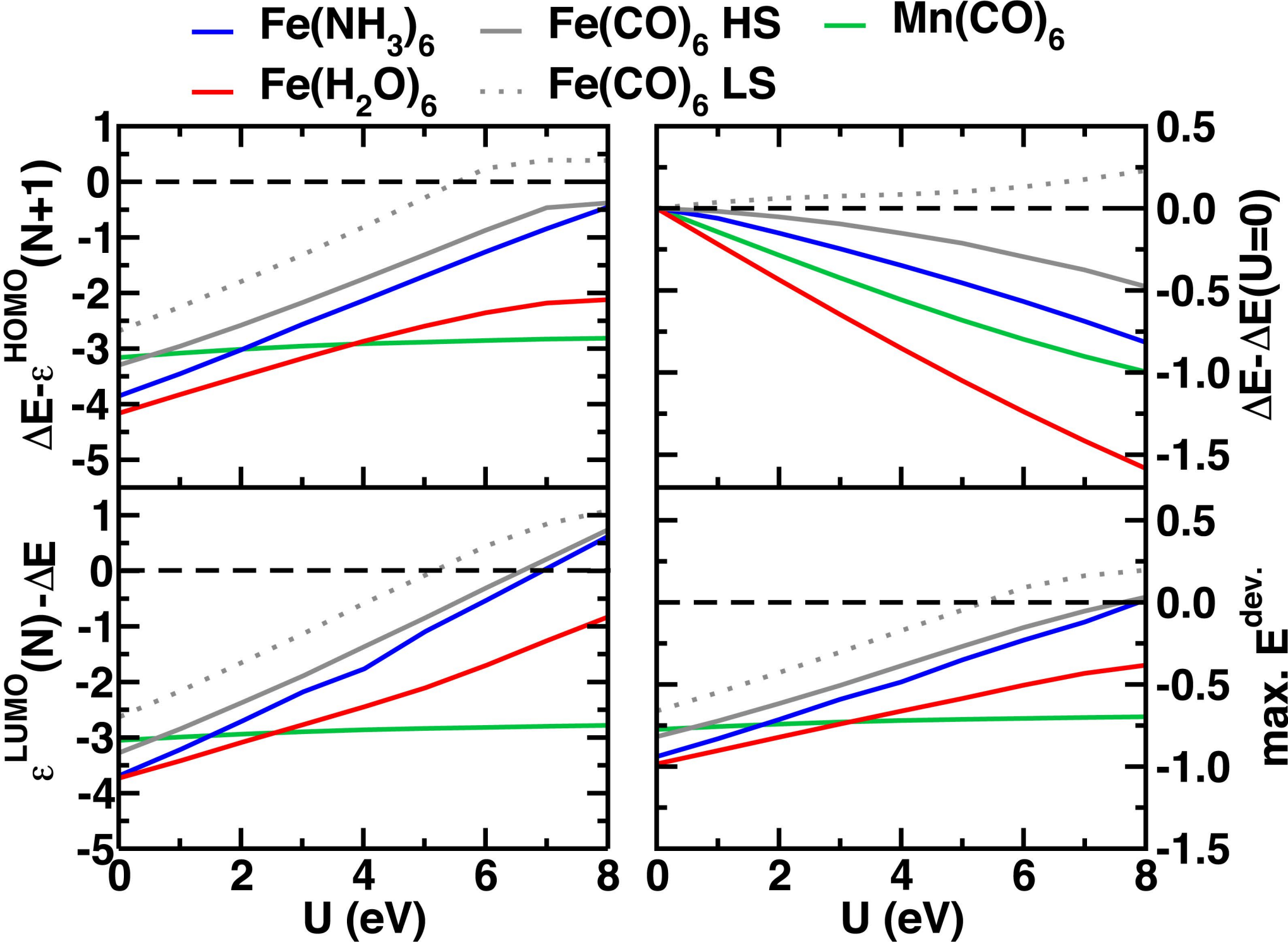
Fe(NH3)6
Fe(H2O)6
Fe(CO)6 HS
Fe(CO)6 LS
Mn(CO)6
ΔE-ε HOMO (N+1)
ε LUMO (N)-ΔE
ΔE-ΔE(U=0)
max. E dev.
U (eV)
U (eV)

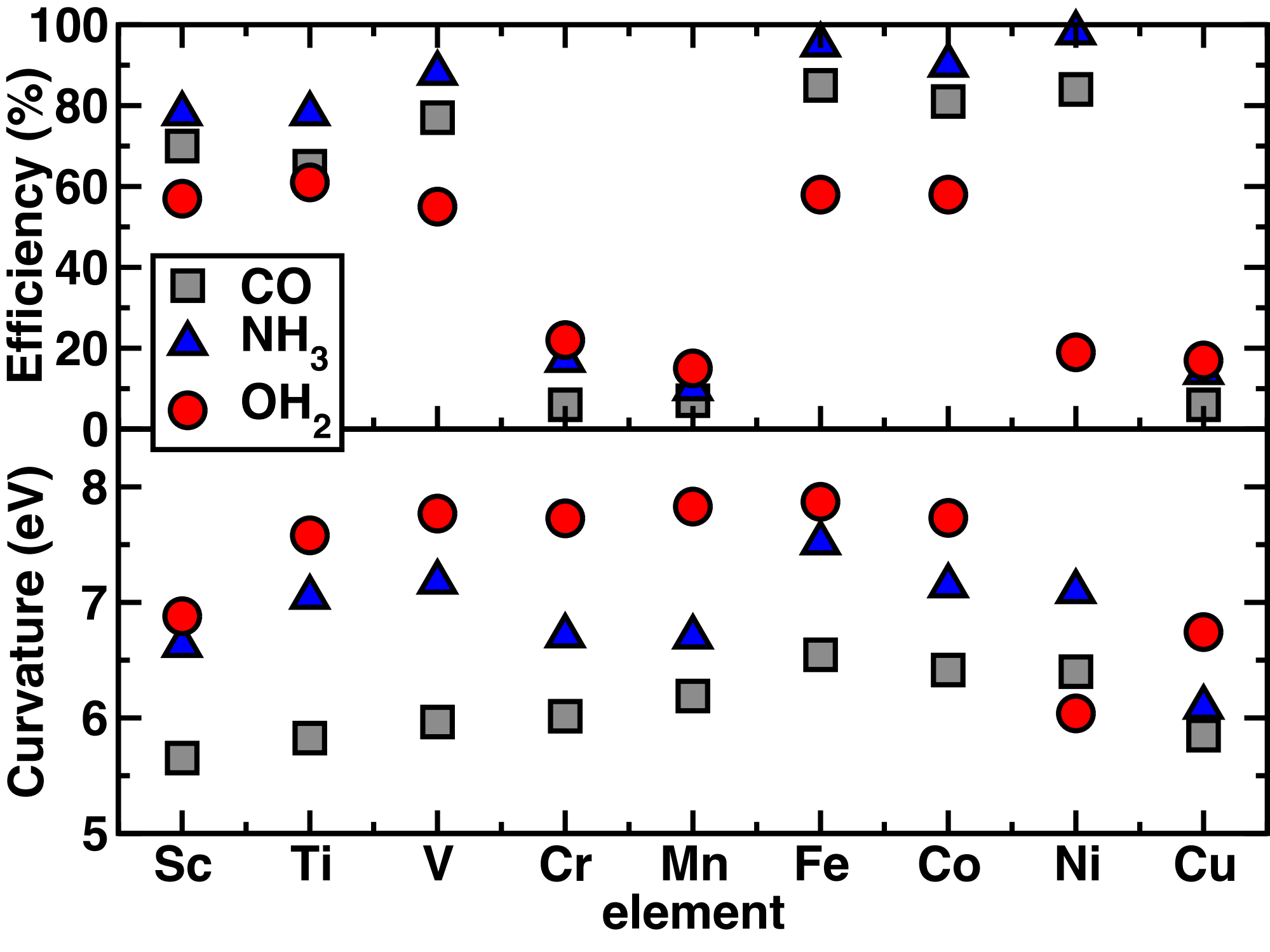
Efficiency (%)
100
80
60
40
20
0
CO
NH3
OH2
Curvature (eV)
8
7
6
5
Sc
Ti
V
Cr
Mn
Fe
Co
Ni
Cu
element

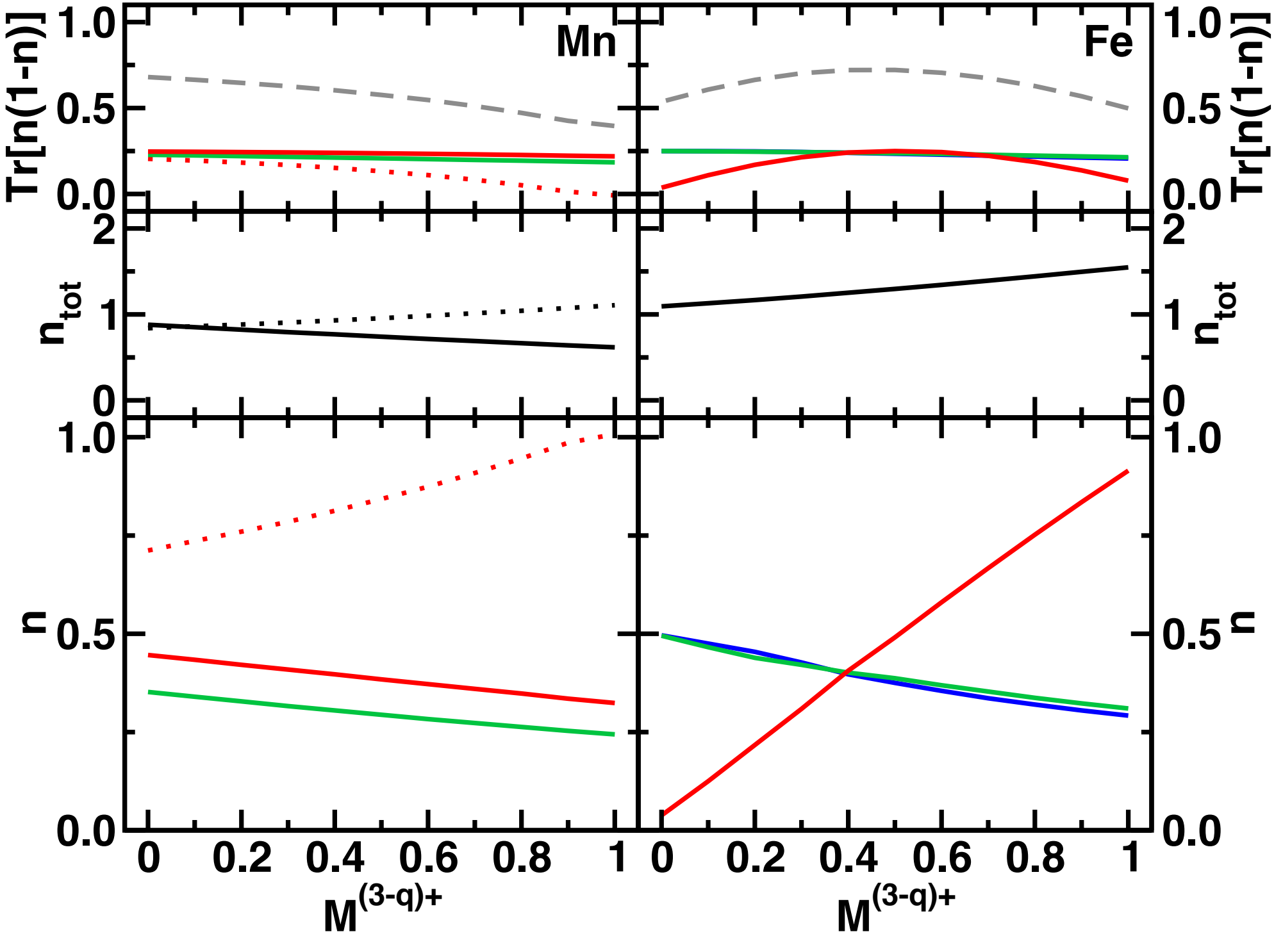
Mn
Fe
Tr[n(1-n)]
Tr[n(1-n)]
n_tot
n_tot
n
n
1.0
0.5
0.0
2
1
0
0
0.2
0.4
0.6
0.8
1
M^(3-q)+
M^(3-q)+

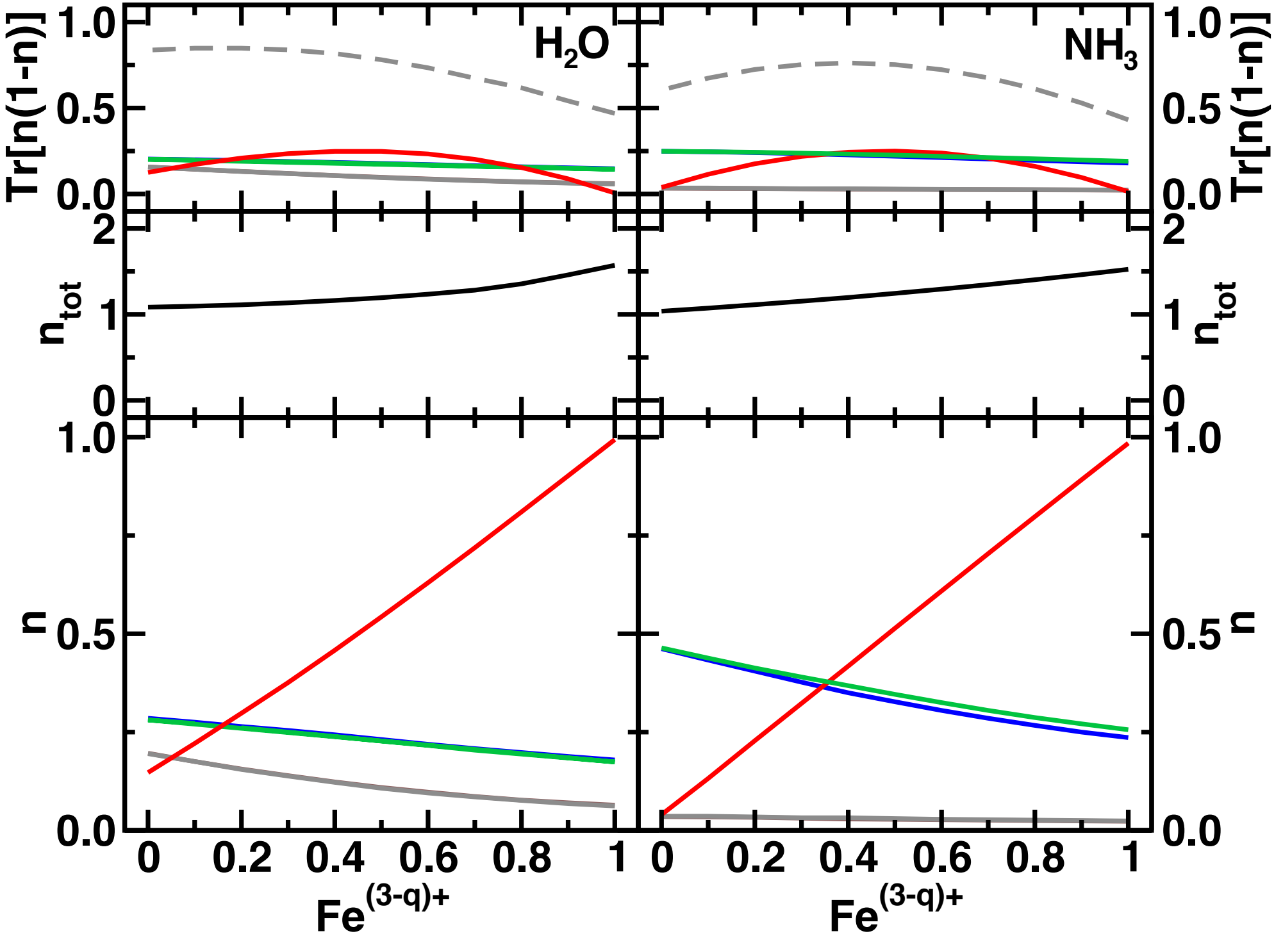
H2O
NH3
Tr[n(1-n)]
n_tot
n
Fe^(3-q)+
0
0.2
0.4
0.6
0.8
1
0.0
0.5
1.0
2

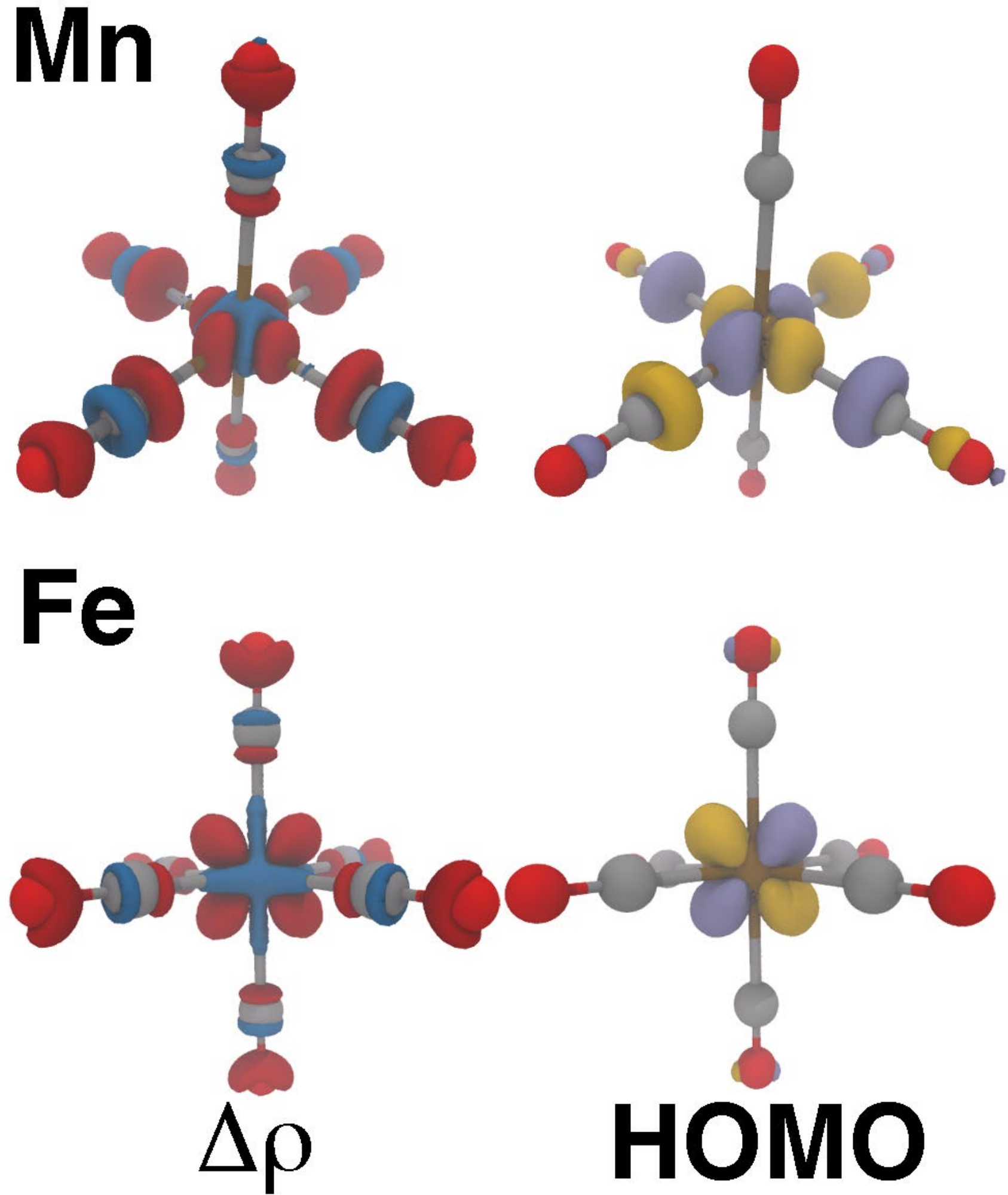
Mn
Fe
Δρ
HOMO

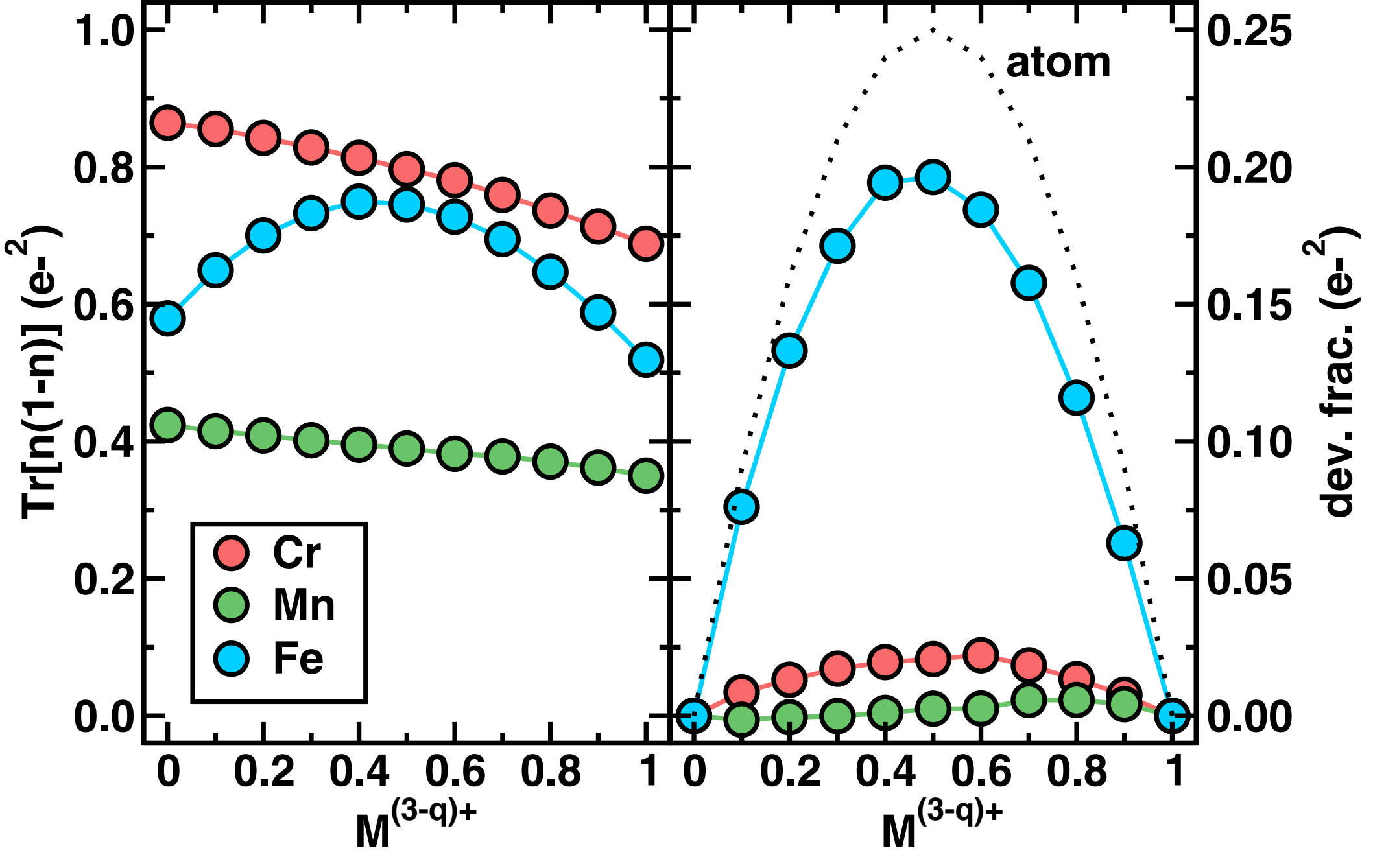
Tr[n(1-n)] (e-2)
dev. frac. (e-2)
atom
Cr
Mn
Fe
M(3-q)+
M(3-q)+
0.0
0.2
0.4
0.6
0.8
1.0
0.00
0.05
0.10
0.15
0.20
0.25
0
0.2
0.4
0.6
0.8
1

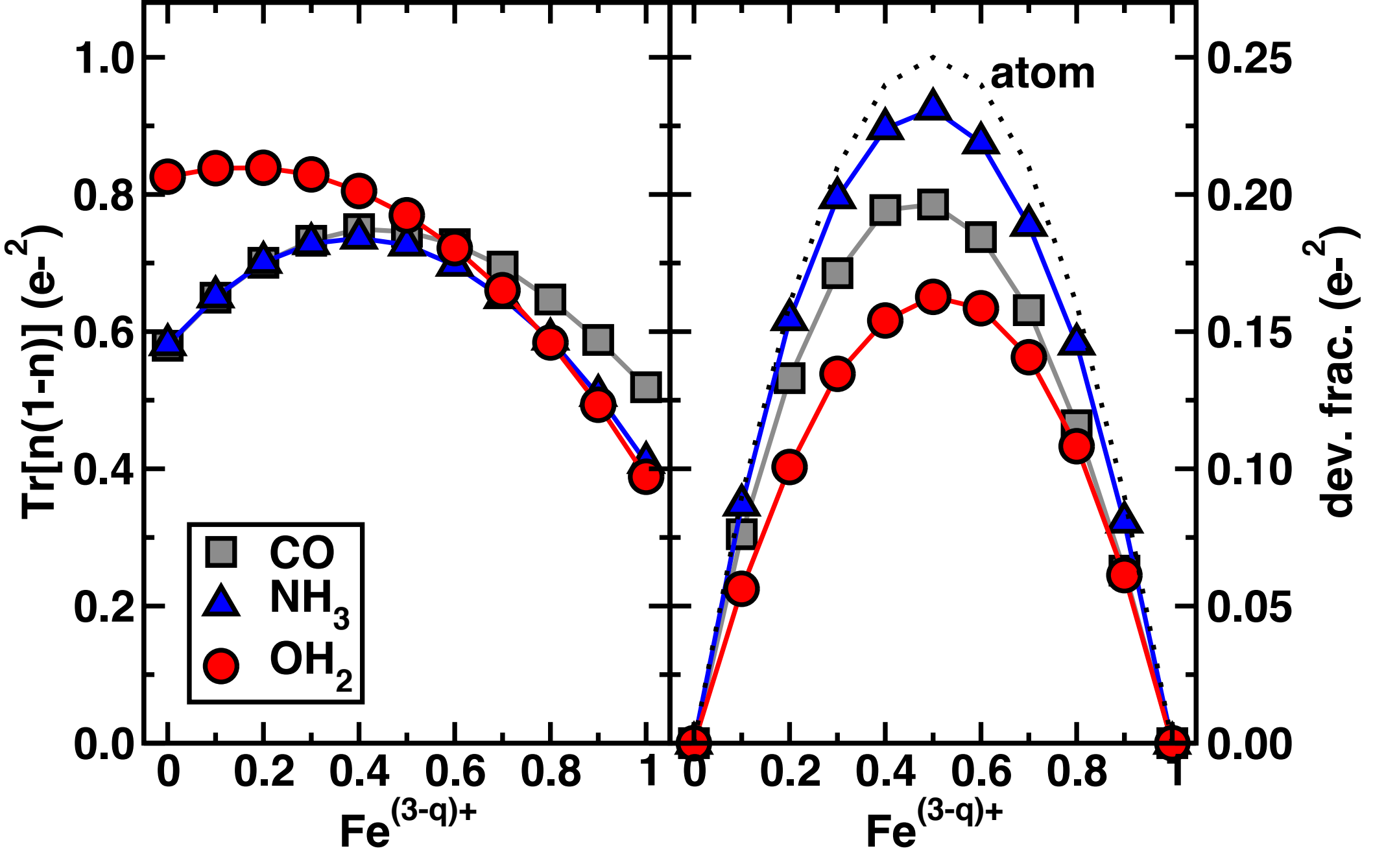
Tr[n(1-n)] (e-2)
dev. frac. (e-2)
Fe(3-q)+
Fe(3-q)+
atom
CO
NH3
OH2
0.0
0.2
0.4
0.6
0.8
1.0
0
0.2
0.4
0.6
0.8
1
0.00
0.05
0.10
0.15
0.20
0.25

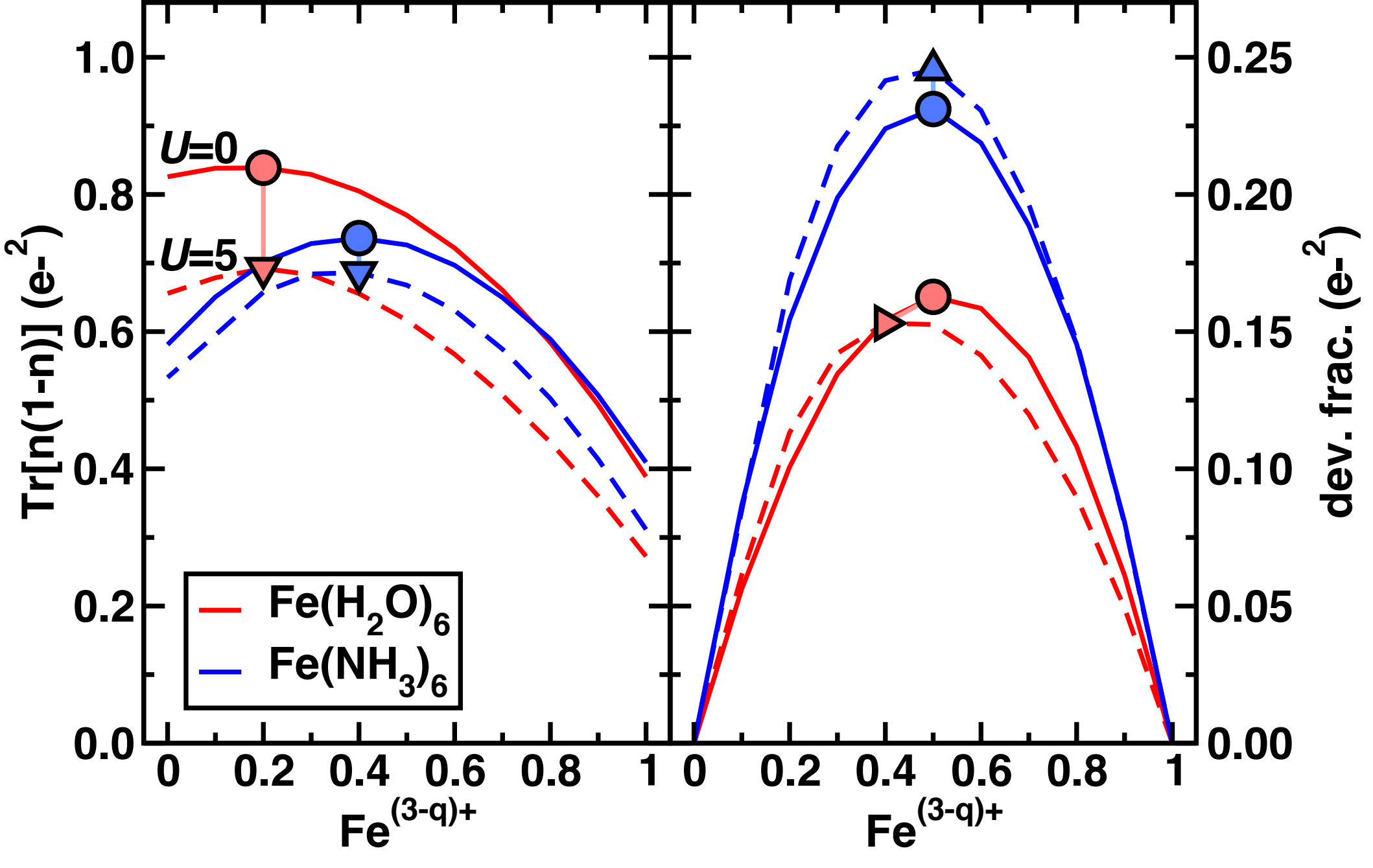
U=0
U=5
Fe(H2O)6
Fe(NH3)6
Tr[n(1-n)] (e-2)
dev. frac. (e-2)
Fe(3-q)+
Fe(3-q)+
0.0
0.2
0.4
0.6
0.8
1.0
0.00
0.05
0.10
0.15
0.20
0.25
0
0.2
0.4
0.6
0.8
1

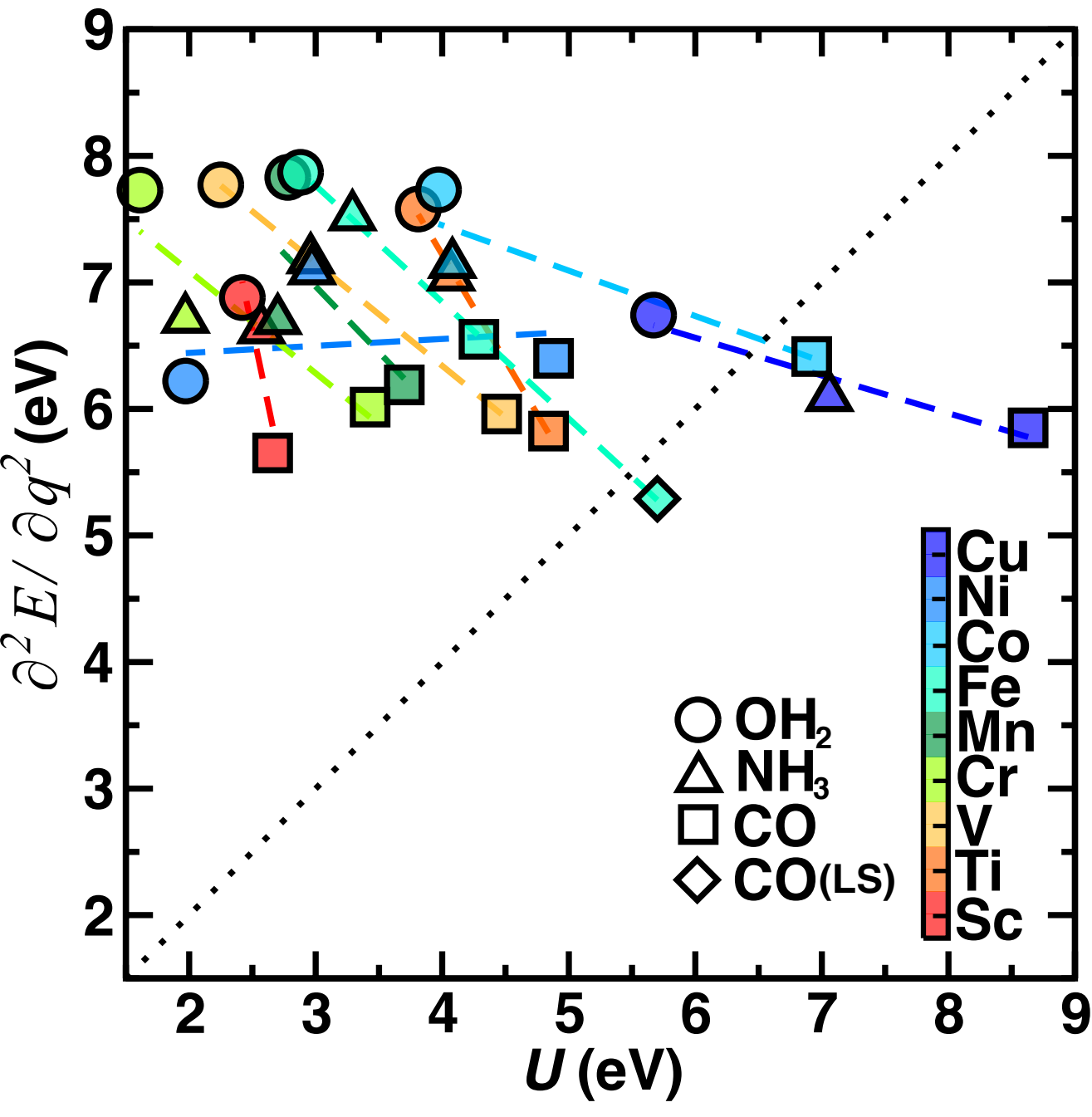
9
8
7
6
5
4
3
2
2
3
4
5
6
7
8
9
$\partial^2 E/\partial q^2$ (eV)
U (eV)
OH_2
NH_3
CO
CO(LS)
Cu
Ni
Co
Fe
Mn
Cr
V
Ti
Sc

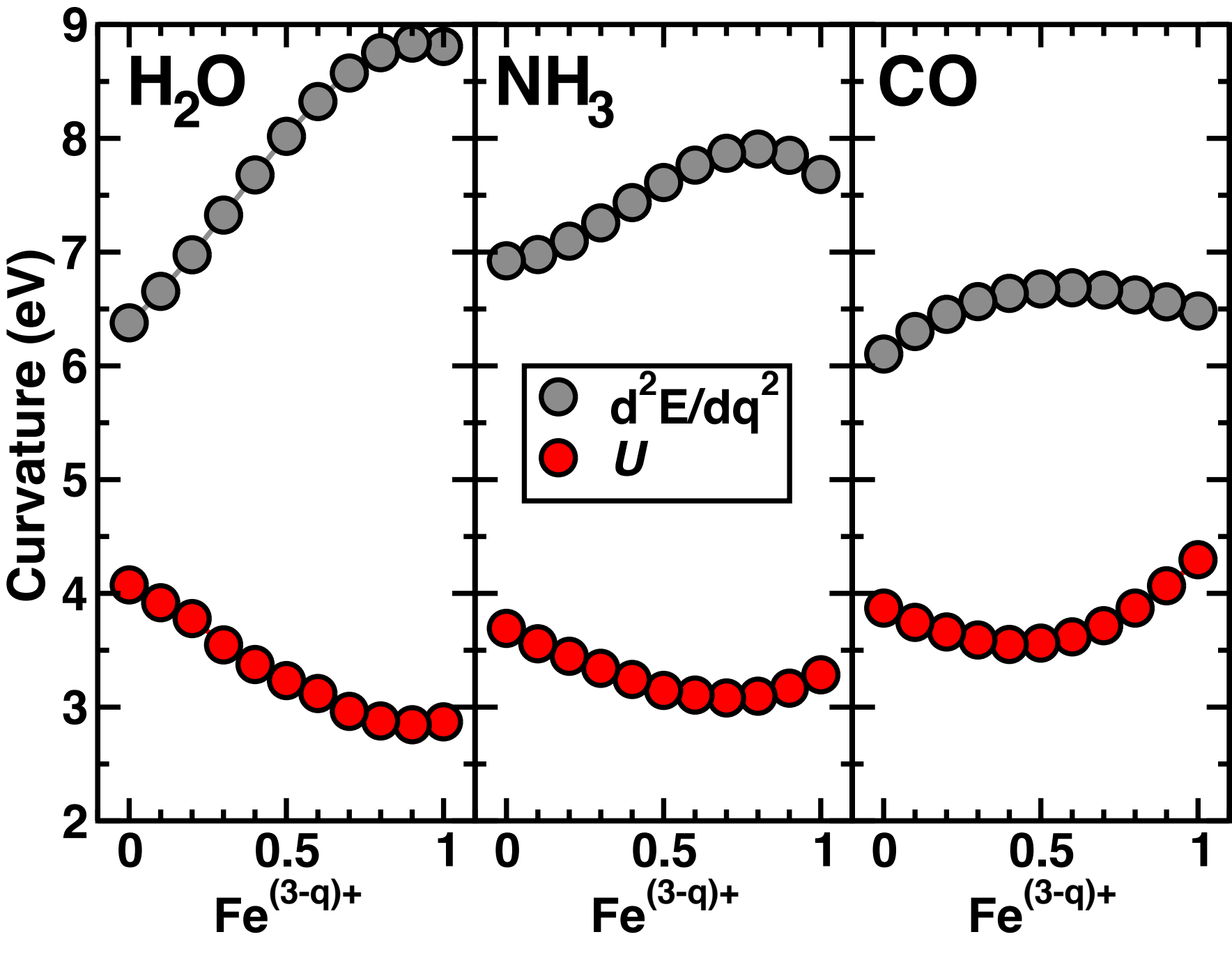
H2O
NH3
CO
Curvature (eV)
d2E/dq2
U
Fe(3-q)+
Fe(3-q)+
Fe(3-q)+
9
8
7
6
5
4
3
2
0
0.5
1
0
0.5
1
0
0.5
1